



The author(s) shown below used Federal funding provided by the U.S. Department of Justice to prepare the following resource:

Document Title: Automated Sperm Detection for Screening and Analysis of Sexual Assault Evidence Samples

Author(s): Pamela Korda, Ph.D., Byeong-Seok Chae, PhD., Ryszard Duszak, Ph.D., Sergio Guevara, Dan Mueth, Ph.D., Evan Tanner

Document Number: 252005

Date Received: November 2018

Award Number: 2011-DN-BX-K562

This resource has not been published by the U.S. Department of Justice. This resource is being made publically available through the Office of Justice Programs' National Criminal Justice Reference Service.

Opinions or points of view expressed are those of the author(s) and do not necessarily reflect the official position or policies of the U.S. Department of Justice.

Automated Sperm Detection for Screening and Analysis of Sexual Assault Evidence Samples

Final Technical Report for NIJ Award 2011-DN-BX-K562

Reporting Period: January 2012 to March 2013

Principal Investigator: Pamela Korda, PhD

Additional authors: Byeong-Seok Chae, PhD
Ryszard Duszak, PhD
Sergio Guevara
Dan Mueth, PhD
Evan Tanner

Submitted on: April 4, 2013

Abstract

In recent years, automation of laboratory practices has been effectively deployed in sample analysis, allowing improved quality control, simpler validation, increased workforce efficiency, lower cost, and higher throughput. In processing forensic samples, automation has played a critical role, focusing on liquid sample handling including DNA extraction, DNA quantitation, and setting up PCR reactions. However, upstream processing steps are still labor-intensive, time consuming, and performed with variability. There are presently few options for automated screening of sexual assault kit elutes for presence of sperm, quantitative cell counting, and precise sperm isolation. Sexual assault evidence samples still require significant manual processing, subject to variability and the negative screening of weakly positive samples. Additionally, commonly used DNA quantitation methods have limited precision, ultimately causing failures in STR profiling.

Arrayx has developed a powerful platform for automated microscopy which leverages machine-vision for object recognition and holographic optical trapping (HOT) for cell manipulation within aqueous cell samples contained in active fluidic disposables. Ongoing work on upstream forensic processing has focused on the use of HOT to isolate individual sperm from the sexual assault samples on this microscopy platform. Our studies have demonstrated that this method is compatible with downstream PCR-based STR profiling.

This report describes the further development of this platform to incorporate hardware improvements and advanced image analysis methods for identification and isolation of sperm. Specifically, the construction of the disposable microfluidic cartridge that is used for fluid handling has been modified to enable more consistent manufacturing and to improve performance. The interface between the microfluidic cartridge and the imaging system has been redesigned for greater stability of focus and better coupling to the external pressure supplies used to control flow. Image analysis routines have been designed to identify sperm in bright-field microscope images, without requiring the use of fluorescent dyes, and work was begun on expanding the capability of these routines to discriminate between sperm and particles of similar appearance, such as yeast.

Table of Contents

Abstract.....	1
Table of Contents.....	2
Executive Summary.....	3
1 Introduction and Background.....	10
1.1 Statement of Problem.....	10
1.2 Review of Literature.....	11
1.2.1 Automated Sperm Analysis with Computer Vision.....	11
1.2.2 DNA Quantitation.....	11
1.3 Rationale for Research and Project Objectives.....	12
2 Methods and Techniques.....	13
2.1 Automated Holographic Optical Trapping Device.....	13
2.1.1 Holographic Optical Trapping.....	13
2.1.2 Actively Pumped Microfluidics.....	16
2.2 Sperm Sample Acquisition.....	17
2.3 Statistical Analysis Methods.....	17
3 Results.....	18
3.1 Microfluidic Chip Improvements.....	18
3.1.1 Development of COC Fluidic Layer.....	18
3.1.2 Optical Clarity of the COC Channels.....	20
3.2 Improvements to the Microfluidic Substage.....	23
3.3 Automated Sperm Identification under Bright Field Illumination.....	29
3.3.1 Identification of Best Focal Plane.....	30
3.3.2 Locally Adaptive Thresholding.....	31
3.3.3 “Three Sigma” Background Correction.....	33
3.3.4 Distinguishing Sperm from Yeast.....	35
4 Conclusions.....	41
4.1 Summary and Discussion of Results.....	41
4.2 Implications for Policy and Practice.....	42
4.3 Implications for Further Research.....	43
5 References.....	45
6 Dissemination of Research Findings.....	47

Executive Summary

Automated Sperm Detection for Screening and Analysis of Sexual Assault Evidence samples

Background: Statement of Problem

Short tandem repeat (STR) analysis has become a powerful and widely used method of forensic DNA analysis, particularly in the case of sexual assault evidence, which often contains both sperm from the perpetrator and epithelial cells from the victim. Acquiring a good STR profile of the perpetrator requires the success of several intermediate steps, such as establishing the presence of sperm in a sample, isolation of sperm from non-sperm entities, DNA extraction from the isolated sperm, DNA quantitation, PCR reaction and STR analysis of the PCR-amplified DNA. Automated computer-vision detection and identification of individual sperm cells in sexual assault kit elutes has the potential to address several shortcomings in current lab workflows, particularly when it is combined with a means of isolating the sperm thus identified from the remainder of the elute, such as holographic optical trapping (HOT). Two of the more important problems are carryover of victim DNA to the sperm DNA fraction and inaccuracies in DNA quantitation. Furthermore, such automation could significantly reduce the amount of manual labor required in processing sexual assault DNA evidence, and facilitate record-keeping. The objective of the research described in this report is to address these needs through the development of automated sperm recognition software for use with a device for automated sample handling and sperm isolation.

Purpose of Research

The work presented here builds upon previous work, which was funded under NIJ awards 2008-DN-BX-K123 and 2009-DN-BX-K260. That work established the compatibility of optical trapping and fluorescent staining of sperm with STR analysis, and supported the development of key components of an integrated device for using holographic optical trapping (HOT) for automated isolation of sperm cells from eluted sexual assault evidence swabs. The research covered under the current grant (NIJ award 2011-DN-BX-K562) was oriented towards making improvements to hardware and developing software for acquiring and analyzing bright-field microscope images in order to identify sperm eluted from mock evidence swabs, alone and in the presence of yeast and other materials likely to be found in forensic swab elutes. It was hoped that obtaining a count of the number of sperm in the output area of the microfluidic device used in the sperm separation would prove to yield a consistent estimate of the quantity of sperm DNA input to the PCR process, thereby complementing or even improving traditional DNA quantitation methods.

Methods:

The hardware system used in this research is an automated platform that combines microfluidics, microscopic imaging, and holographic optical trapping. Several elements of this device were developed under the auspices of NIJ award 2009-DN-BX-K260, and are documented in the final technical report for that grant (see Reference 12).

We provide here a summary of key laboratory methods used in the present research:

- **Holographic Optical Trapping:** Optical trapping is a technique for manipulating microscopic particles, such as cells, using strongly-focused laser beams. Holographic optical trapping (HOT) is a variation of optical trapping that uses a phase mask (hologram) to shape a laser beam's wave-front in order to create many optical traps from a single laser beam. One implementation of the technique uses a computer-controlled liquid-crystal spatial light modulator (SLM) to generate the necessary phase masks and update them in real time, thus enabling computer-controlled, simultaneous, three-dimensional manipulation of multiple particles.
- **Microfluidics:** "Microfluidics" is a catch-all term for the study of, and techniques used to manipulate, fluids on very small scales. A microfluidic device, also referred to as a "chip," typically comprises a series of micro-scale fluid channels, along with means of moving fluid through those channels. For an application such as sperm isolation, microfluidic chips provide the link between the separation abilities of optical trapping and the necessary inputs and outputs accessible to pipettes and other sample transport mechanisms.
- **Sperm sample acquisition:** Hardware testing and image-analysis software development both used samples eluted from mock forensic swabs provided by Orchid Cellmark. Most tests used sperm eluted from swabs containing sperm only, although some of the later work involved material eluted from swabs containing both sperm and epithelial cells, or sperm and yeast. Elution was performed using a proprietary protocol supplied by Orchid Cellmark.
- **Software:** The hardware platform was operated using custom software developed in-house using National Instruments' LabVIEW. Image acquisition and analysis used LabVIEW and the NI Vision add-ons. Statistical analysis of image data was performed using R version 2.15.1.

Results: Microfluidic Chip Improvements

The microfluidic cartridge, or "chip," is a key component of the sperm isolation system. It is where the observation, measurement, and isolation of the sperm from the remainder of the elute take place, and forms the interface between the microscopic sperm contained in the elute and the macroscopic tools used to manipulate them. Our chip consists of a series of 100-micron-scale channels. The channels incorporate pneumatically controlled

valves that control the flow of liquid and particles in those channels. At the beginning of this research phase, the channels for our chips were constructed of a glass substrate bonded to laser-cut silicone. In order to address an ongoing problem with bubble formation and to reduce the complexity of the chip manufacturing process, we replaced the silicone-and-glass channel assembly with a single piece of molded cyclic olefin copolymer (COC). This change also improved the consistency of chip manufacturing.

Moving to COC-molded channels introduced a new difficulty, in that the molded COC did not have good optical clarity, as the glass-bottomed chips did. Since optical clarity is important for both imaging and optical trapping of particles inside the channels, this was problematic. The source of the problem was the mold from which the channels were produced. Several modifications to mold design were attempted, and we eventually were able to achieve greatly improved optical quality through fabricating the mold from a harder aluminum alloy than we had previously used, which could be polished to a higher quality. Achieving better polishing required implementing a new, more complex, polishing method.

An additional step taken to reduce bubble formation in the channels during long-time operation was to coat the silicone membrane that forms the active portion of the in-channel valves with parylene, in order to reduce the porosity of the membrane.

Results: Improvements to the Microfluidic Substage

In our automated sperm isolation device, an off-the-shelf translation stage is used to move the microfluidic chip relative to the imaging and optical tweezing elements. The custom chip is coupled to the off-the-shelf translation stage via a substage that is inserted into the main stage. In addition to holding the chip in place, this microfluidic substage connects the chip's pneumatic layer to the valve manifold and to the external pumps that provide positive and negative pressure for driving fluid flow within the channels. During the present research phase, the microfluidic sub-stage has gone through two upgrades to remedy issues seen in the previous design.

The previous design used pneumatic clamps attached the sub-stage to push down on a metal plate that, in turn, clamped the microfluidic device to the sub-stage and sealed the chip's air ports with the sub-stage's mating air ports. This design provided tight pneumatic coupling between the chip and the valve manifold, but the bottom fluidic layer of the device, i.e. the location of the sperm relative to the microscope imaging plane, was observed to migrate vertically over time. The effect was large enough to cause significant defocusing of the imaging system over the course of processing a sample. As a result, images were not consistent, and the imaging system's autofocus routine had to be run frequently. This effect was not observed in samples which were not clamped, and so the cause of the drift was believed to be deformation of the microfluidic device itself caused by the high clamping force needed to seal the air ports between the chip and the sub-stage.

Several design revisions were applied, ultimately resulting in a design that included a single monolithic silicone gasket to seal the chip to the pneumatic pressure lines, and spring-loaded clamps to hold the chip in place. When this design was implemented, the rate of focus drift was observed to be around half of what it had been when using the pneumatic-clamp design. This was a substantial improvement, and likely the best that could be achieved without a complete hardware redesign.

Results: Automated Sperm Identification under Bright Field Illumination

During our previous development phase, computer identification of sperm was aided by the use of fluorescence microscopy. A fluorescent intercalating dye was introduced to the elute, prior to inspection. This dye, propidium iodide, tagged the nuclei of the cells present in the sample, including the sperm. Inspection of the sample was performed using standard fluorescence microscopy techniques. In the resulting images, cells appeared as bright red spots on a black background, and sperm were distinguished from epithelial cells on the basis of spot size. One of the main objectives of this phase was to implement imaging and image analysis methods that did not depend on the use of fluorescent dye, so that sperm could be identified under ordinary bright field microscope illumination.

Since the appearance of a cell in a microscope image depends on the location of the focal plane relative to the cell's position, the first task was to identify the focal position where sperm had the most distinctive appearance. This was done by looking at the contrast between sperm cells and background. The focal position with the highest contrast was found to be 7 μm above the bottom of the microfluidic channel. At this position, sperm appeared as bright oblong spots, surrounded by a dark "shadow."

The next step was to implement a thresholding procedure to identify bright image features that would be considered as candidates for identification as sperm. The stock algorithms in the NI Vision 2010 package were found to produce unreliable results. Instead, we analyze the intensity histogram of an image, and select the upper (bright) tail of the intensity distribution. This approach resulted in correct identification of all sperm cells in our test images, with no spurious identifications.

Distinguishing sperm from the background is a necessary capability, but it is not the whole of the problem. A real forensic evidence swab does not only contain sperm, but may include a number of other components, such as epithelial cells from the victim or possibly the assailant, or yeast, which grows naturally inside the human vagina. While epithelial cells are much larger than sperm and appear significantly differently under bright-field illumination, yeast can have similar size and shape to sperm. Misidentification of yeast cells as sperm would increase processing time, and introduce error into any attempt to estimate the human DNA quantity in the processed sample by counting the number of "sperm" in the output area.

We used mock samples containing sperm and yeast to examine the morphological properties of both cell types, and to identify parameters that could be used to distinguish

sperm from yeast in our microscope images. We considered the following quantities, and found that they all differed significantly between yeast and sperm:

- Hydraulic radius: this is the area of the shape, divided by its perimeter
- Waddell Disk Diameter: this is the diameter of a circle with the same area as the particle
- Ratio of equivalent ellipse axes: this is the ratio of major axis to minor axis lengths of an ellipse that has the same area and same perimeter as the shape
- Elongation factor: this is the ratio of the largest distance between any two points in the shape to the length of the short side of a rectangle having the same area and same perimeter as the shape
- Heywood circularity factor: this is the perimeter of the shape, divided by the circumference of a circle of the same area. It is a measure of circularity
- Area: the number of pixels in the shape

Unfortunately, these conclusions are based on very small numbers of yeast and sperm, because our research program was terminated before we were able to gather and analyze more data. However, we hope that our observations may point a direction for future researchers.

Conclusions: Summary and Discussion of Results

As laid out previously, one major objective for our research project was to develop methods for computer identification of human sperm eluted from a sexual assault evidence swab under bright-field microscopy. These methods, along with associated hardware improvements, were to be implemented on our automated holographic optical trapping device for isolating sperm from other components of the elute. Our follow-up objective was to be investigating the potential for using the imaging techniques to complement or improve upon current DNA quantitation techniques by counting the number of sperm in the output area of the device.

The hardware challenges proved to be more important than we had anticipated, and thus required a greater proportion of resources and time to resolve. When we moved from glass-bottomed microfluidic chips to chips with COC-molded channels, the optical quality of the COC channels was mediocre. Several design iterations were required to obtain a satisfactory manufacturing process for the mold from which the COC chips were made. In the final process, the mold was machined from one-inch thick surface-ground blocks of Alumold 500 aluminum, and polished to an optical finish using techniques derived from Reference 28.

We also had to correct a problem with our automated microcopy system, where the imaging plane of the microscope systematically drifted away from the lower surface of the channels. The cause of this effect was determined to be an excess of clamping force used to hold the chip in place and couple it to the pneumatic system for controlling the microfluidic valves. This force caused the acrylic body of the chip to deform over time, resulting in vertical displacement of the fluidic channels relative to the imaging plane. An

new clamping system was designed and built, which exerted considerably less force on the chip. When the new clamping system was used, the focus was still found to drift over time, but at one half the rate that had been previously observed.

Once these hardware challenges were addressed to our satisfaction, we were able to proceed with acquiring good bright-field images of eluted sperm and developing image-analysis software techniques for identifying sperm and distinguishing it from other particles that might be found on a sexual assault evidence swab, such as yeast. However, we were not able to make further progress with the image analysis work, or to attempt DNA quantitation through image analysis, because our research and development program was terminated prior to the end of the funding period.

Conclusions: Limitations

The main technical limitations on our research were hardware and sample related. Over the course of the current research phase, it has become clear that we have reached the limit of our present hardware's capabilities. This hardware had originally been developed as a general-purpose instrument, to which adaptations were made over time to make it suitable for sperm isolation. Any significant further progress towards a commercial device would require production of a second-generation instrument designed with the forensic application in mind. Regarding limitations due to samples, all of our work to date has used mock forensic swabs supplied by Orchid-Cellmark. These swabs contain sperm, sperm and yeast, or sperm and epithelial cells, and have sufficed for early-phase development. However, these mock swabs are not necessarily characteristic of real evidence swabs collected from sexual assault victims. The most obvious difference is that real evidence swabs are collected from a victim's body, and are thus likely to contain a wider variety of contaminants than samples produced under controlled laboratory conditions. Were this project to continue, it would be necessary to partner with a working forensic laboratory which could, hopefully, supply more realistic test samples.

Beyond technical limitations, the results of the project, and our ability to address our initial goals, were hampered by the fact that our research program has been terminated and our division closed. The final decision was made in early 2013, but it was preceded by the ending of other projects being pursued by Arrayx, and the transfer of another project to a different division of our parent company. The effect of these business decisions on our project was a sharp reduction in resources and personnel we could call on to support the forensics project. The cumulative effect was that we were able to accomplish considerably less than we had envisioned when our proposal was submitted to the NIJ in 2011.

Implications for Criminal Justice

Our informal discussions with forensic scientists suggest that there is a great deal of interest in the prospect of an automated device for high-purity sperm isolation from sexual assault evidence. A device that is sufficiently fast and affordable would reduce or eliminate the need for differential extraction, which in turn would improve lab efficiency

by freeing workers for other tasks. The capability to observe a sample throughout its processing would allow for improved and automated record-keeping. Knowing the number of sperm cells that have been isolated, and which are to be used for STR profiling would enable more precise estimation of the optimal quantity of PCR reagents needed, and thus improve the probability of obtaining a good result.

Although we will not be continuing this research program ourselves, we present here some recommendations and suggestions for future researchers who may wish to pursue similar work. Development of a robust computer-vision method for identifying sperm eluted from an evidence swab is aided by having a solid, reliable hardware platform. If we were to have continued this project, one of the first objectives would have been to design and produce a new, integrated hardware system designed specifically for the sperm-isolation application. Such a device would have enabled us to partner with a working forensics laboratory, thereby gaining insight into laboratory workflows and the types of samples typically encountered. This, in turn, would have informed the design and production of a commercial instrument.

Our work on developing image analysis routines for identifying sperm in bright field microscope images was in its early stages when work was stopped. We hope that the example presented in this report will point the way towards development of a more generally-applicable approach. The first step should be acquiring a large number of images of sperm alone, yeast alone, epithelial cells alone, and images of mixtures of those components. By analyzing these images, one could identify the combination of morphological parameters that is most effective in identifying sperm. It may prove to be the case that the best approach is to use a combination of bright field imaging and fluorescence imaging to identify all components of interest in a swab elute.

A final step would be to implement holographic optical trapping to trap and move sperm identified by a reliable sperm-recognition routine. The sperm thus isolated could be counted, extracted, and then subjected to traditional DNA quantitation methods. This would provide valuable insight into the possibility of supplementing traditional quantitation with sperm counts in order to better estimate the quantity of PCR reagents to be used in amplification prior to STR analysis.

1 Introduction and Background

1.1 *Statement of Problem*

Forensic DNA analysis for human identification relies upon the ability of short tandem repeat (STR) analysis to accurately distinguish and identify genetic material from different individuals. STR analysis has become a powerful and widely used method of forensic DNA analysis, particularly in the case of sexual assault evidence, which often contains both sperm from the perpetrator and epithelial cells from the victim. Achieving a good STR profile of the perpetrator requires the success of several intermediate steps, such as establishing the presence of sperm in a sample, isolation of sperm from non-sperm entities, DNA extraction from the isolated sperm, DNA quantitation, PCR reaction and STR analysis of the PCR-amplified DNA. However, the implementation of STR in a common lab workflow suffers from several shortcomings. Two of the more important problems are carryover of victim DNA to the sperm (perpetrator's) DNA fraction¹ and inaccuracies in DNA quantitation. Large errors in DNA quantitation often lead to PCR failures because the reagents used in the PCR process are either in large excess for the amount of DNA actually present to be amplified or in much lower amounts than necessary to carry out the amplification. This can also indirectly lead to waste of reagents.

Automated, computer-vision detection and identification of sperm in sexual assault kit elutes has the potential to address both of these problems. An accurate sperm count based on machine vision can lead to improved estimates of how much DNA can be expected post-extraction. Computer-based cell identification can also assist with the automation of sperm isolation using techniques such as holographic optical trapping (HOT). As an additional benefit, automated detection and identification of sperm could significantly reduce the amount of manual labor—and therefore cost—involved in screening forensic evidence for the presence of sperm.

To date, automation efforts towards forensic analysis of sexual assault evidence have found limited use and have remained primarily focused on downstream processing such as DNA extraction or PCR reaction setup. However, data tracking from start to finish can be facilitated if a robust algorithm can be developed which will address the existing drawbacks in sample handling and manual processing from an early stage. The objective of the research described in this report is to address those needs through the development of automated sperm recognition software that is flexible, accurate and fast, coupled with a device for automated sample handling and sperm isolation.

1.2 Review of Literature

1.2.1 Automated Sperm Analysis with Computer Vision

Automated sperm analysis software has been developed outside the field of forensics, typically measuring morphology and motility to infer fertility, usually for *in vitro* fertilization (IVF) programs.² Scientists in the field of andrology have developed an automated semen analyzer^{3,4} to improve efficiency and decrease variability in results due to different operators. However, the analysis of sperm quality using these automated methods still showed substantial difference when different technicians operated them or when different staining methods were used. The criteria used in such sperm detection for IVF mostly looked at fresh sperm with intact tails, and occasionally at the morphology of the sperm head. Furthermore, the samples used were more homogenous than those present in a forensic sample. Additionally, in andrology applications, statistically sound assessment of healthy sperm morphology could be based on analysis of few, not necessarily all, sperm on a slide. The sperm detection software developed for use in andrology were primarily focused on assessing the quality of sperm, whereas in the forensic context it is the quantity of sperm available in a sample that is of interest. While both disciplines require shape analysis using image processing, the criteria needed for andrology versus forensics are quite different. Robust automated sperm detection software intended for forensics use has not been available, and forensic labs rely on time-consuming and labor intensive manual searches for sperm for initial screening of every sexual assault evidence sample.

1.2.2 DNA Quantitation

Common DNA quantitation methods used by forensic laboratories have been found to yield large variations in measured DNA content, which often leads to unsuccessful PCR and hence failures in STR profiling for human identification. A study conducted by the US National Institute of Standards and Technology (NIST) to better understand the variability in DNA quantitation techniques, reported up to 10-fold variation in the reported amount of DNA.^{5,6} For a 1 ng DNA sample supplied to 74 laboratories in an inter-laboratory study, the returned values ranged from 0.1-3 ng while the median value was close to 1ng. Different methods are employed for DNA quantitation in forensic labs which include fluorescence readout from an intercalating dye such as picogreen,⁷ real-time PCR such as the quantifiler kit⁸ or the Alu assay.⁹ and end-point PCR such as the BodeQuant assay.¹⁰ The limits of detection are quite different for each of the methods and the volumes required by the kits range from 2-10 μ l. These quantitation uncertainties are likely amplified by other factors including contaminating DNA from sources other than sperm and the presence of various chemicals used in the extraction process.

1.3 Rationale for Research and Project Objectives

Our previous research, funded by NIH awards 2008-DN-BX-K123¹¹ and 2009-DN-BX-K260¹², was directed towards developing a prototype system for automated isolation of sperm from mixed cell solutions eluted from a variety of mock evidence swabs, and developing a disposable cartridge for sample handling and recovery of the sorted sperm fraction. The ultimate goal of our work was to create a viable and cost-effective technology which could be automated for the identification and physical separation of sperm from other components in a forensic sexual assault sample.

To this end, we have developed a system that combines microscopy, image acquisition and analysis, holographic optical trapping, and microfluidics. Key components and functionalities of the device are described in Reference 12, and in Section 2. During development, identification of sperm was aided through the use of a fluorescent nuclear dye. However, realizing that our staining protocol might not be universally compatible with forensic lab workflows, we determined to improve the system's hardware and software so that sperm can be identified using ordinary bright-field imaging methods.

Beyond utility in cell sorting, automated sperm identification can be applied to both the screening and quantitation stages of evidence processing. Automated identification of sperm can reduce or eliminate the need for manual inspection of eluted samples. At the other end of the process, precise counting of the number of sperm present—which will be passed on for PCR amplification and STR profiling—can aid in quantitation. Quantitation based on sperm counting employs the knowledge that a diploid human cell contains ~6pg genomic DNA and that 1 ng of genomic DNA corresponds to approx 333 copies of each locus to be amplified. By counting the number of sperm in a sample, one has a more precise estimate of the amount of sperm DNA available for amplification. Automated sperm detection can thus reduce total time in sample processing and assist in reducing the backlog¹³ of sexual assault forensic evidence.

The goals for the work described in this report were:

1. Improving the hardware of our automated microscopy and microfluidics platforms to a level capable of producing clear, high-quality bright field images of sperm and other material contained in the mock swab elutes
2. Develop robust methods for acquiring and analyzing images produced by our hardware system, to identify sperm eluted from mock evidence swabs, alone and in the presence of yeast and other materials likely to be found in forensic swab elutes
3. Investigate the degree to which counting of sperm in the output chamber of a microfluidic chip can yield a consistent estimate of the quantity of sperm DNA input to the PCR process.

2 Methods and Techniques

In this section, we describe key methods that we used to pursue the project objectives, as summarized in Section 1.3. We describe the apparatus used in our development efforts, and key technologies it employs. We also briefly summarize statistical methods used in conjunction with image analysis in Section 3.4. Note that methods and techniques developed as part of our research objectives are described in the results section, Section 3.

2.1 Automated Holographic Optical Trapping Device

During previous phases for this project, we have developed an automated device that integrates fluid handling, optical microscopy, image analysis, and optical trapping, with the objective of isolating sperm eluted from mock forensic swabs. Details of our development efforts can be found in the final technical report for NIJ award 2009-DN-BX-K260.¹² Figure 1 illustrates the process from start to finish. Sperm and other material is eluted from a swab (Figure 1a-b). A portion of the elute is then injected into an actively-pumped microfluidic cartridge (Figure 1c), which is in turn placed in the instrument. The instrument contains optical components for illuminating and imaging the contents of the cartridge (Figure 1d). Elute is pumped into a “separation channel” (Figure 1e) and imaged. After computer image analysis, particles that are identified as sperm are captured with optical traps (Figure 1f) and moved to an output channel (Figure 1g). Once a sufficient number of sperm have been collected, the sperm are pumped to an output area, where they can be collected for further analysis (Figures 1h-i). Note that many of the development efforts discussed in this report do not require running the entire process from start to finish, and that the pumping and imaging routines in particular were operated on their own while pursuing objectives relating to those functions alone.

A photograph of the device can be seen in Figure 2. Additional details about its components can be found in Reference 12.

Two technologies that are of critical importance to this process are holographic optical trapping and the actively pumped microfluidic cartridge.

2.1.1 Holographic Optical Trapping

Optical trapping, invented in 1970 at Bell Labs,¹⁴ uses strongly-focused beams of coherent light to form traps that can hold and move microscopic particles. Over the years, it has found many applications in cell biology,¹⁵ including studies of sperm motility,¹⁶ functionality of motor proteins,¹⁷ and of DNA structure and conformation.¹⁸ Since biological materials generally do not absorb light in the near-infrared wavelength range (approximately 700-1500 nm), lasers operating in this range are preferred for optical trapping of cells. Previous research performed in our laboratory found that prolonged optical trapping using 1064 nm wavelength laser light does not have a deleterious effect on STR profiling of trapped sperm.¹¹

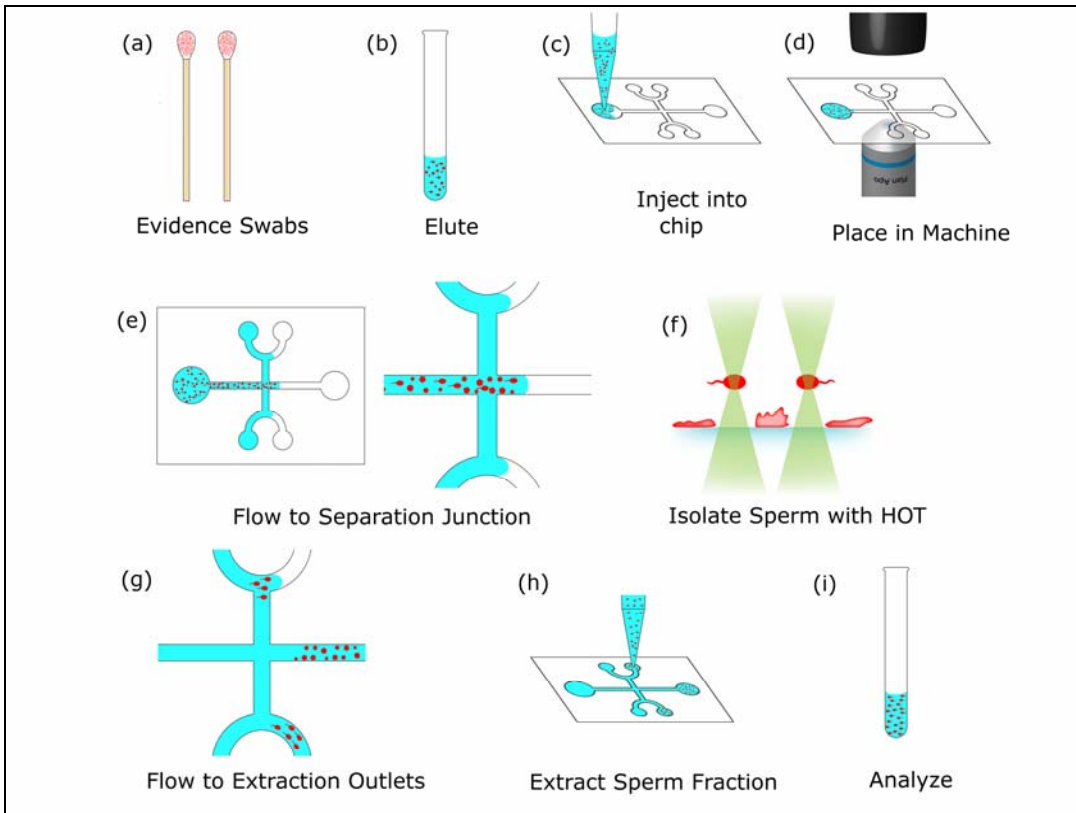


Figure 1 Process for automated isolation of sperm from sexual assault evidence.

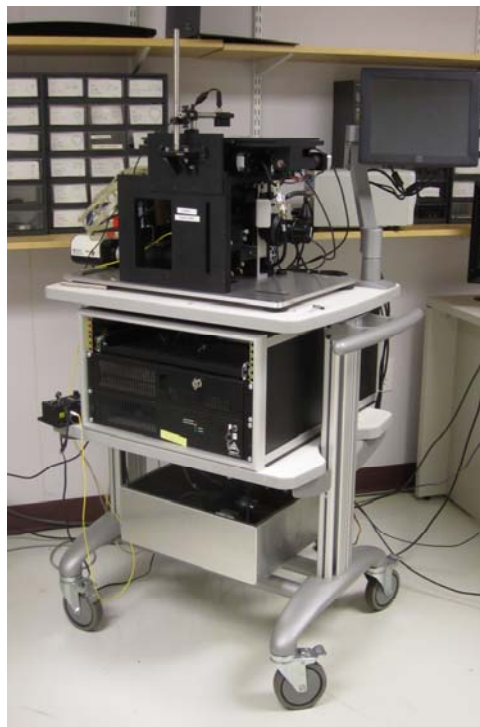


Figure 2 Device for automated isolation of sperm from sexual assault evidence, comprising imaging, optical trapping, and fluid-handling systems.

Holographic optical trapping (HOT) was developed by David Grier and Eric Dufresne at the University of Chicago in 1997.¹⁹ HOT is an extension of optical trapping in which a phase mask (hologram) is used to sculpt the wave-front of the trapping laser, splitting the single beam into many optical traps. By using a liquid-crystal spatial light modulator (SLM) to generate the phase masks,²⁰ Arryx is able to produce multiple optical traps that can be independently located and controlled in three dimensions. SLMs are available that have refresh rates of up to 100 frames/second and that are able to withstand several Watts of CW laser light for extended periods of time.²¹ Using Arryx's HOT API, new holograms can be calculated in milliseconds, enabling real-time control of the optical traps.

Figure 3 shows schematically how an SLM is employed to generate multiple, arbitrarily located traps from a single laser beam. Holographic Optical Trapping (HOT) using a spatial light modulator (SLM): collimated laser light is incident on the face of a liquid-crystal SLM, which imposes a phase profile on it. The light is then transferred to the back aperture of a microscope objective lens, using a series of lenses and mirrors. The objective lens focuses the light into a number of optical traps, that can be manipulated by changing the SLM's phase profile. Images of the trapped particles in the sample are collected by a CCD camera. Coupled with a CCD camera and computer-based image processing, HOT forms the basis for a machine-vision guided system that can automatically execute sophisticated manipulations and isolations.²²

For detailed information about traditional optical trapping, we recommend Reference 15. For discussion of holographic optical trapping, please consult Reference 22.

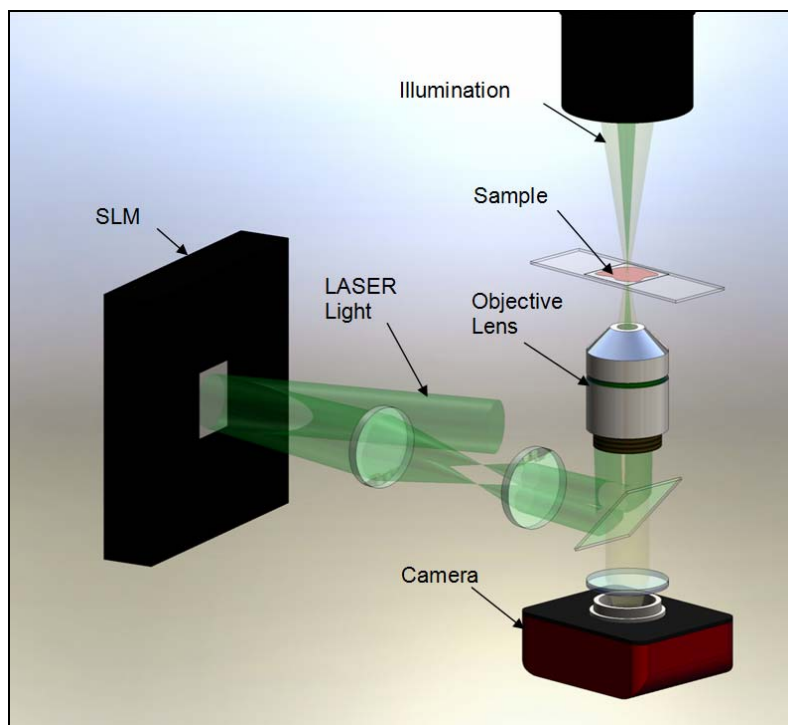


Figure 3 Holographic Optical Trapping (HOT) using a spatial light modulator (SLM)

2.1.2 Actively Pumped Microfluidics

The term “microfluidics” refers to the manipulation of fluids on nanoliter and smaller scales. The typical microfluidic platform is the so-called “lab on a chip”—a system of micro-scale channels that is custom-designed to move fluids in a controlled manner for a particular application. A lab-on-a-chip device usually comprises a means of introducing fluids and microscopic particles to the device, a means of moving fluids through the channels, and application-specific components such as detectors, filters, or fluid outlets.²³ Additionally, it is desirable to include a means of monitoring the state of the fluid and particles inside the channels. This can be done by incorporating optically clear regions into the chip design, and observing these regions with an optical microscope.

One of the major challenges of the previous phase of this project was the development of a microfluidic chip that contained active fluid control, in which sample flow can be automated and controlled by the computer. Development of this chip involved multiple iterations of channel design, material selection, and sample treatments, before a device that performed acceptably well in most areas was achieved. Although there were further improvements to make, we have largely succeeded in creating a design that:

1. Is compatible with optical trapping
2. Has adequate and robust fluid manipulation capabilities, which will enable correct sample injection and separation
3. Allows for adequate sample throughput over the course of processing a sample

The microfluidic devices that we have developed use the technique of on-chip, active valving and pumping developed by Grover and Mathies.²⁴ These active devices are based on valves incorporated into the microfluidic channels. The valves are controlled by pressure applied through a second “pneumatic” layer which is separated from the fluid layer by an elastomer membrane. Pressure in the pneumatic layer is supplied via a pair of diaphragm pumps and a computer-controlled valve manifold.

To enable easy modification of channel designs, the chips used during the previous development phase were constructed from five layers of material, as shown in Figure 4. The bottom layer is a 150 μm thick glass microscope coverslip, which is plasma-bonded to a laser-cut silicone layer that holds the fluidic channels. A second silicone layer separates the fluidic channels from a laser-cut PMMA layer which contains the pneumatic channels. Finally, a second PMMA layer seals the pneumatic channels, and contains inlets and outlets for test samples, as well as connections for the Lee valve manifold. Although the devices thus constructed functioned largely as desired, they had some problems that promised to become significant when the chip was operated over extended periods of time. The two main issues were sperm adhering to the channel walls and formation of air bubbles inside the channels. One of the first objectives of this project phase was to address these problems through improved chip design.

For details regarding the design, construction, and operation of these chips, the reader is referred to Reference 12.

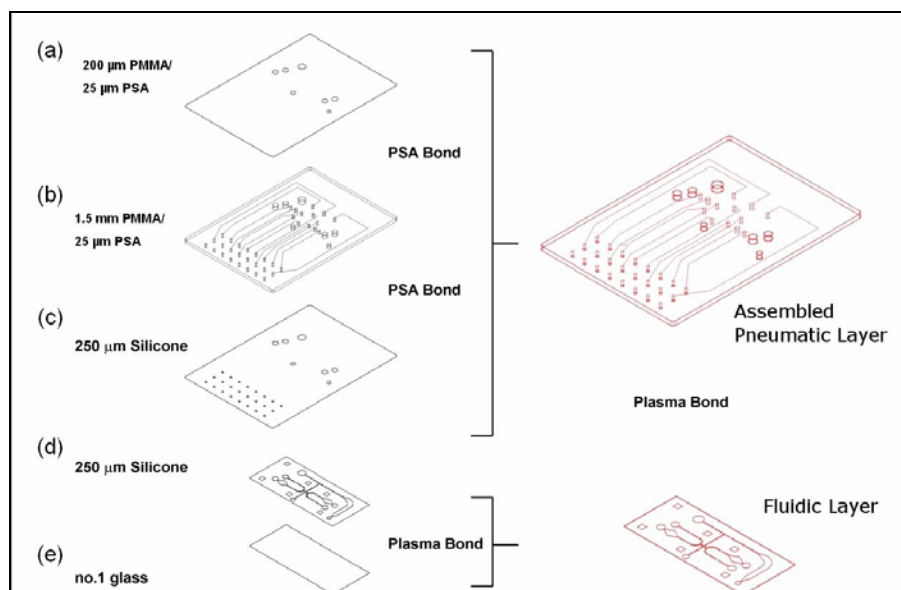


Figure 4 Fabrication of a five-layer active microfluidic device. The pneumatic layer (a-c) comprises three sections that are bonded with pressure sensitive adhesive. The fluidic layer (d-e) consists of two sections that are bonded using plasma oxidation (plasma bond).

2.2 Sperm Sample Acquisition

All of the work presented in this report that required the use of sperm was performed using mock forensic samples acquired from Orchid Cellmark (now a division of LabCorp). Microfluidic testing used sperm eluted from swabs containing sperm only. Image analysis work used sperm-only samples, samples containing a mixture of sperm and epithelial cells, and samples containing a mixture of sperm and yeast. Elution of the swabs was performed using a proprietary protocol supplied by Orchid Cellmark.

2.3 Statistical Analysis Methods

In some of the image analysis work described in this report, we employed common statistical techniques. Specifically, the Welch two-sample t-test was used to identify characteristics and metrics that differentiate images of sperm from images of yeast. All statistical analysis was performed in R version 2.15.1.²⁵

3 Results

The majority of work described in this report falls into two general categories. First, there were hardware improvements to the microfluidic device and to the integrated system for HOT-based sperm isolation that were developed during the previous phase.¹² Some of these improvements were directed toward improving the overall reliability and performance of the system, and included significant changes to the manufacturing process for the microfluidic chip. These developments are discussed in Section 3.1.1.

Other hardware changes were necessary to produce the high-quality images of the material in the microfluidic channels. This was a prerequisite for the second area of work, which was to develop image-analysis techniques for identifying sperm in images produced using bright-field microscopy. It necessitated further modification of the chip manufacturing process and a number of changes to the interface between the microfluidic chip and the sperm isolation device. These developments are discussed in Sections 3.1.2 and 3.2.

A key goal for this research phase was to develop relatively quick and reliable image-analysis methods for identifying sperm in bright-field images. Although efforts in this area were ongoing, significant progress was not made until the hardware issues were resolved. Although the software we developed for this purpose is particular to our hardware platform, the methods employed in creating it are more widely applicable, and are described in Sections 3.3 and 3.4.

3.1 Microfluidic Chip Improvements

The microfluidic cartridge, or “chip,” is a key component of the sperm isolation system. It is where the observation, measurement, and isolation of the sperm from the remainder of the elute take place, and forms the interface between the microscopic sperm contained in the elute and the macroscopic tools used to manipulate them. Our chip, depicted in Figure 5, consists of a series of 100-micron-scale channels and the means to control the flow of liquid and particles in those channels. Sample fluid containing sperm flows through the channels, controlled by valves incorporated into the channels. A comprehensive description of principles of operations of this chip can be found in the Final Technical Report for NIJ award 2009-DN-BX-K260.¹²

3.1.1 Development of COC Fluidic Layer

At the beginning of the research phase documented in this report, the chips were fabricated as described in Section 2.1 and shown in Figure 4. Although this design operated fairly well, long-time operation—such as would occur while processing an evidence sample—resulted in bubble formation within the channels. These bubbles both impeded the smooth flow of fluid through the channels, and also had the potential to interfere with imaging, depending on the locations of the bubbles. Additionally, sperm tended to stick to the glass surface that formed the channel bottom. While this could be

ameliorated by coating the microscopic channels with Pluronic® F-127, manufactured by BASF, doing so was a laborious process, and was not scalable to the higher volumes of device production we anticipated needing for this phase of development.

The material properties of the silicone used to form the channel walls and membrane were believed to be the cause of the bubble formation. Specifically, the fact that silicone is relatively porous resulted in small volumes of air leaking into the channels through the silicone, and when the microfluidic device was operated for 20 minutes or more, this resulted in visible bubbles inside the channels. This problem was addressed on two fronts. First, the silicone-and-glass assembly used for the channel walls and substrate were replaced with a single piece of molded plastic. The plastic chosen for this role, cyclic olefin copolymer (COC) is commonly used for biological and chemical microfluidic applications.²⁶ Using COC instead of a glass substrate also obviated the need for Pluronic coating of the channels. The second modification for reducing bubble formation was to coat the silicone membrane separating the pneumatic and fluid layers of the microfluidic device with parylene (Specialty Coating Systems, Indianapolis, IN). The parylene coating—applied to one side of the membrane prior to chip assembly--fills the pores in the silicone and thereby prevents air from penetrating into the fluid layer, while leaving the membrane flexible enough to perform its function.

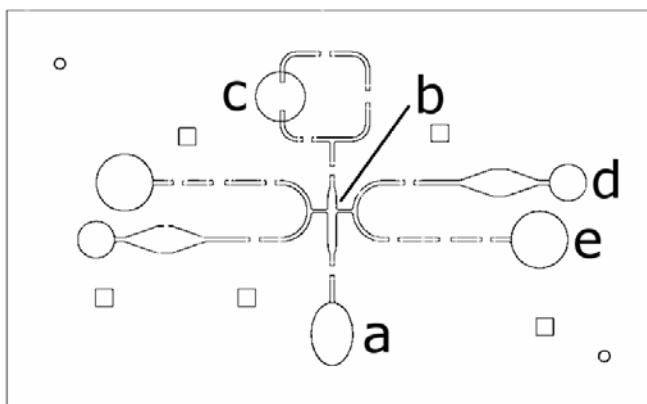


Figure 5 Microfluidic channel pattern for sperm isolation: (a) Inlet for eluted sample, (b) Separation area, (c) Recirculating reservoir, (d) Sperm recovery outlet, (e) Inlet for buffer. The gaps in the channels are valves. The isolated features are registration marks. In later versions, the widening of the channel near the outlet (d) was eliminated, in order to improve recovery efficiency of the isolated sperm.

The compression mold for the COC fluid layer was designed in SolidWorks, and machined on a programmable CNC mill. The channel pattern is shown in Figure 5; two sets of channels can be produced per mold. Molds were machined from aluminum (7075 aluminum alloy) and steel (PX5 steel), and then polished so that the resulting channels would have the optical clarity necessary for imaging and trapping the sperm. The assembly process for the COC-based microfluidic devices is similar to that used for the silicone-and-glass devices discussed in Section 2.1. First, the layer containing the pneumatic channels is assembled from two pieces of laser-cut acrylic, bonded together with pressure-sensitive adhesive (PSA). The silicone membrane layer—coated with

parlylene—is then bonded to the acrylic, again using PSA. The parlylene-coated side faces the pneumatic channels. Following the method described by Sunkara in Reference 26, the COC fluid channel layer is made from the mold, coated with aminopropyltriethoxysilane (APTES), and treated with oxygen plasma (SPI Plasma Prep II). The COC layer is then immersed in water containing APTES. The combined silicone-pneumatic layer is aligned with and plasma-bonded to the COC layer.

Approximately 20 microfluidic devices constructed using this process were tested for bubble formation during fluid flow through the channels. Fluorescent microspheres were used to visualize flow, and fluid was pumped in the channels for 90 minutes. Under these test conditions, bubble formation is greatly reduced, compared to the previous design, although it is still not completely eliminated.

3.1.2 Optical Clarity of the COC Channels

As stated in the previous section, we initially attempted using both aluminum and steel to fabricate molds for the COC channels. Both materials proved to have substantial flaws. Due to the relative softness of aluminum, it could not be polished to as high a quality as desired, and the resulting channels, while usable, contained artifacts produced by imperfections in the mold features corresponding to the channels. The steel, on the other hand, could be polished more thoroughly, but the thermal properties of steel resulted in difficulties with the thermal-press molding process. We therefore switched to a harder aluminium alloy, to obtain the thermal properties of an aluminum mold, while allowing for a higher degree of surface polishing.

Developing a good mold-polishing procedure proved to be essential for creating chips with good optical clarity. The initial polishing procedure was based on methods recommended by Engis Corporation for polishing steel molds.²⁷ During this polishing process the polishing stones and diamond polishing compounds were lubricated and thinned with Engis Hyprelube. The polished surfaces produced by this process did not have a perfectly mirrored surface, but one that had some diffusion and a “blurry” appearance. Microfluidic channels produced from such molds proved to have microscopic scratches and other artifacts, which interfered with image analysis and recognition of sperm contained within the channels. An example of such a channel, imaged with bright-field microscopy, can be seen in Figure 6. Note that this channel does not contain any solid material—all of the features seen in Figure 6 are on the channel surface. This uneven surface texture at a fine scale was determined to be produced during the final polishing steps when the finest diamond compounds are used. It was therefore necessary to find a superior polishing method.



Figure 6 Surface imperfections in a molded COC microfluidic channel, viewed with bright-field microscopy.

A number of polishing procedures were tested via trial and error. The best results were obtained using an adaptation of a process described in an article on the MoldMaking Technology website.²⁸ This article recommends a process for polishing aluminum that contains several alterations to the previous polishing method. Only a subset of those changes could be accommodated by the unique design of the microfluidic mold. The most significant of these is using ethanol as a lubricant and thinner.

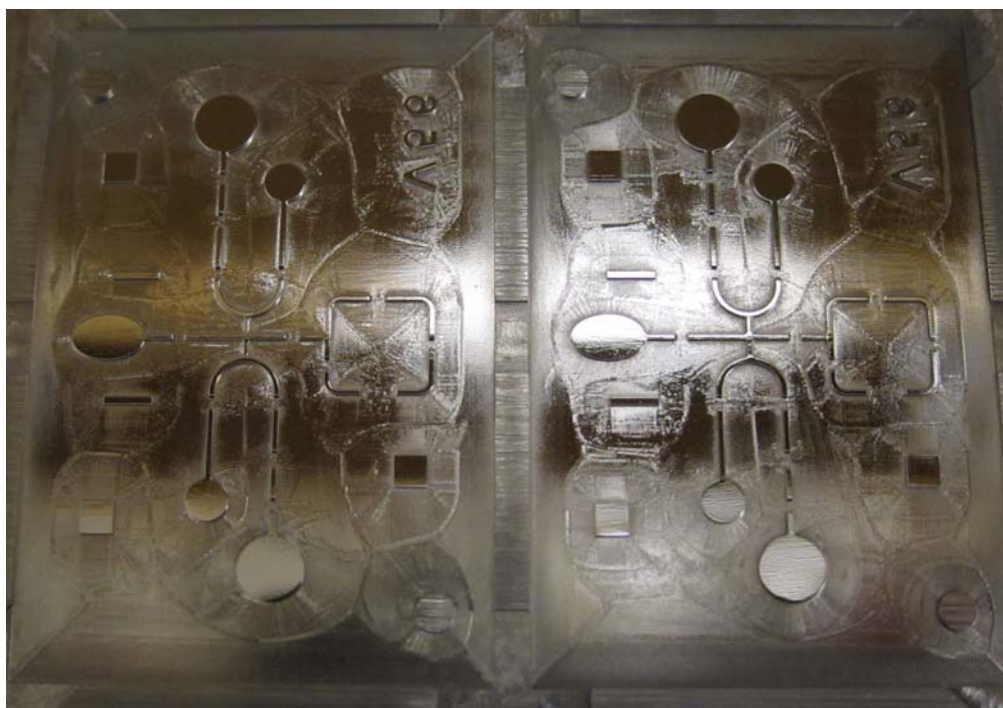


Figure 7 Aluminum mold for microfluidic channels, polished using the method derived from Reference 28.

Figure 7 shows the polished surfaces on a mold made using the preferred polishing method. A mirror-like finish is evidenced by the reflection of the light on the right-side oval. The blurriness observed in the previous molds' polish is not evident. Note that some ripples on the polished surfaces are observable. Such ripples may have been present previously but were obscured by the blurriness of the reflection in the previous mold. The ripples and any issues with flatness are controlled in the early polishing steps by stoning and using larger-grit diamond compounds. They may be due to insufficient flatness of the grinding stones used in the first stages of the polishing process, or due to the stoning and polishing process itself. The MoldMaking article suggests rotating the stoning and polishing direction by 30-degree increments. We used 90-degree increments instead of 30-degree ones because it is easier to accommodate those angles with the layout of the microfluidic channels and features in the mold. If an even higher degree of polishing is found to be needed in the future, it may be necessary to add features to the mold to accommodate rotation of the polishing and stoning by 30 degrees.

However, the ripples on the polished surfaces occur on a length scale that is significantly larger than the field of view of our instrument. Thus, these features do not have an observable impact on the quality of images taken of samples contained in microfluidic channels produced by this mold. Figure 8 shows a microscope image taken of a sperm sample inside a microfluidic device produced from a mold polished with our preferred method. It can be seen that the background is smooth and even. Such images are necessary for development of the sperm-recognition image analysis routines discussed in Section 3.4.

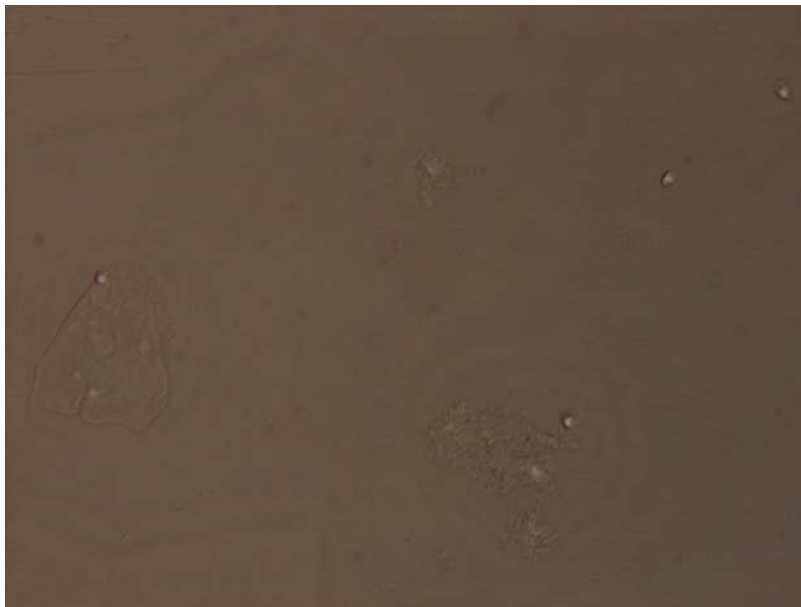


Figure 8 Microscope image of sperm and epithelial cells, in a microfluidic channel produced by the mold in Figure 7. The smooth background is indicative of the high quality of the mold polishing.

3.2 Improvements to the Microfluidic Substage

In our automated sperm isolation device, an off-the-shelf XY translation stage (Prior Scientific H117) is used to move the microfluidic chip relative to the imaging and optical tweezing elements. The custom chip is coupled to the off-the-shelf translation stage via a substage that is inserted into the main stage. In addition to holding the chip in place, this microfluidic substage connects the chip's pneumatic layer to the Lee valve manifold and to the external pumps that provide positive and negative pressure for driving fluid flow within the channels. Figure 9 contains a rendering of the substage, valve manifold, and microfluidic chip, and Figure 10 shows an image of the substage mounted in the Prior Scientific translation stage.

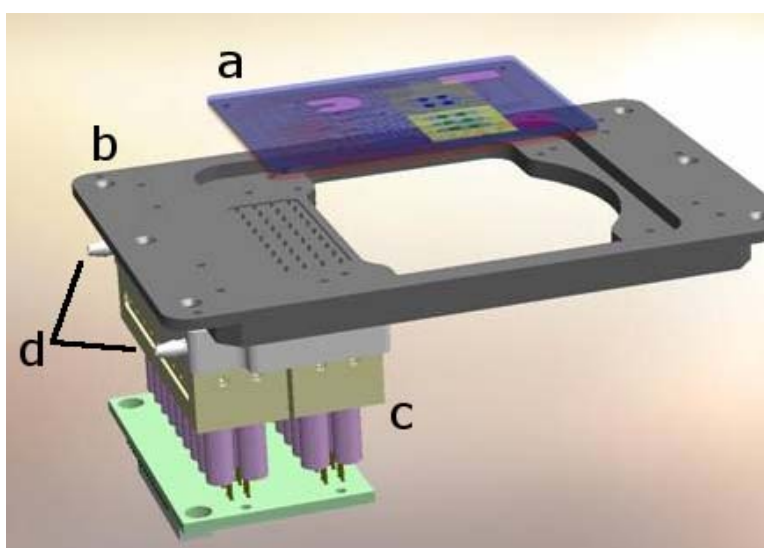


Figure 9 Microfluidic substage assembly. The microfluidic chip (a) is held in the substage (b) and through it is connected to the valve manifold (c). The valve manifold contains connections (d) for positive and negative pressure sources.



Figure 10 The microfluidic substage mounted on the XY translation stage. The valve manifold is out of sight, underneath the translation stage.

During the present research phase, the microfluidic sub-stage has gone through two upgrades to remedy issues seen in the previous design. The previous design used pneumatic clamps (Carr Lane 400 Series 100 lb Air-Powered Clamps) attached the sub-stage to push down on a metal plate that, in turn, clamped the microfluidic device to the sub-stage and sealed the chip's air ports with the sub-stage's mating air ports. This design is shown in Figure 11.

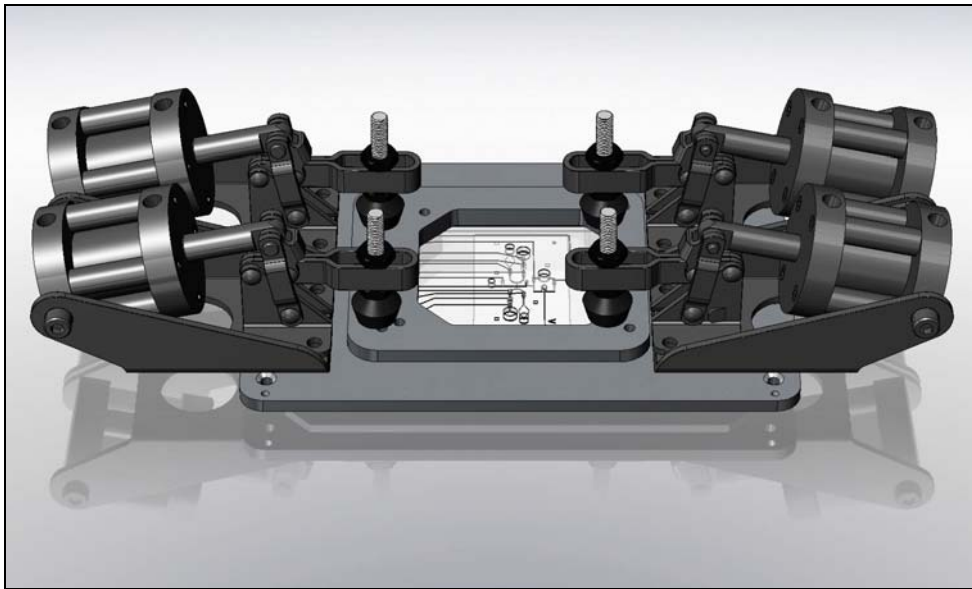


Figure 11 Microfluidic substage prior to upgrades, shown with clamps closed.

Although this design provided tight pneumatic coupling between the chip and the valve manifold, the sub-stage design was found to have a serious problem that interfered with imaging of sperm inside the microfluidic channels. Specifically, the bottom fluidic layer of the device, i.e. the location of the sperm relative to the microscope imaging plane, was observed to migrate vertically over time. The effect was large enough to cause significant defocusing of the imaging system over the course of processing a sample. As a result, images were not consistent, and the imaging system's autofocus routine had to be run frequently. These effects greatly increased processing time, and decreased the reliability of the sperm-identification software. This was found to be the case even when using fluorescence microscopy to image the sperm, a method in which the appearance of the sperm is more robust to small degrees of defocusing than is the case with bright-field imaging.

Because this drift was not observed in samples which were not clamped, we hypothesized the cause of this effect to be deformation of the microfluidic device itself when it was clamped to the sub-stage. The root cause was the high clamping force needed to seal the air ports between the chip and the sub-stage. The microfluidic device has 24 pneumatic ports in an 8 x 3 array which must align with corresponding ports on the sub-stage. The 24 ports on the sub-stage consist of 24 pins that insert into the chip, as shown in Figure 12. The silicone mid-layer of the chip acts as a gasket, which is compressed by the clamps to form a seal between the ports. This method of alignment and sealing required

large clamping forces to align the chip's ports to the pins and form an air-tight seal. Each pneumatic clamp had approximately a 1 psi air pressure to 1 lb of clamping force ratio at the position the clamps were used. Over 20 psi of air pressure was used to activate the clamps, providing over 20 lbs of force at each clamp for a total of over 80 lbs of force clamping down on the chip.

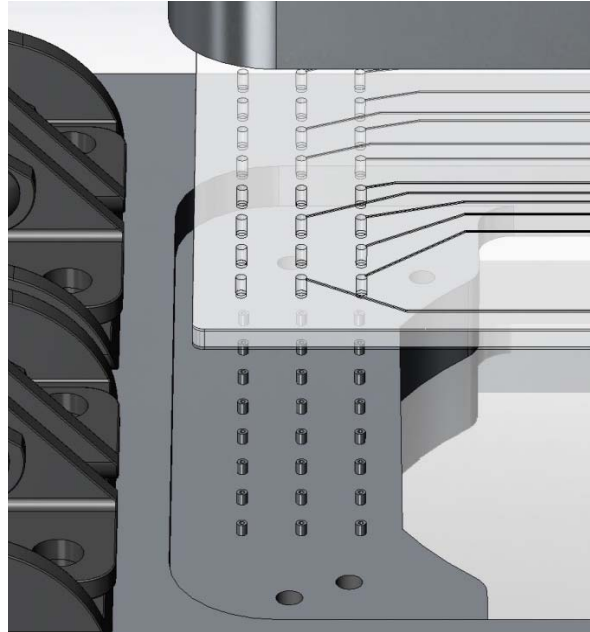


Figure 12 Interface between chip and substage (exploded view)

In order to reduce the force to which the chip was subjected, the interface between the sub-stage and chip ports was redesigned to produce an air-tight seal between device and substage, while using significantly lower clamping force.

The first sub-stage revision, shown in Figure 13, aimed to reduce the clamping force to the smallest amount necessary for the stage and chip to function. A gasket was introduced between the sub-stage and microfluidic device, and the clamping mechanism was redesigned. The minimum clamping force is determined by the pressure being applied at the interface between the substage and chip air ports. The maximum pressure in the air lines is 1 psi, therefore allowing for a safety factor, the pressure the gasket should exert is at least 2 psi. A closed cell silicone foam (Bisco HT-870) was chosen that could be compressed by a small amount and seal the ports with 4 psi. Because of the proximity of the ports to one another, and to ease installation, the gasket was designed as a monostructure to seal all the 24 ports rather than have an individual gasket for each port. The area of the gasket determines the clamping force needed. With an area of 0.8 in², the new gasket needed only 3.12 lbs of force to form the seal. This represented a reduction of over 76 lbs in clamping force, compared to the previous design.

The microfluidic device itself was secured to the sub-stage via a pressure plate, as in the previous design. However, instead of the pneumatic clamping system, simple manual spring clamps were designed to hold the pressure plate onto the chip. The clamps

consisted of steel linear shafts that screwed into the sub-stage with Delrin plastic clamps that slid along it. The clamps had force applied to them by a compressed spring located in between the clamp and nuts at the top of the shafts. The nuts could be adjusted to reduce or increase the clamping force. The springs were chosen to apply a static load that would counter the pressure from the gasket in compression. The pressure plate was also modified to allow a ball on the bottom of the clamps to sit in predefined positions, to ensure that clamping was consistent.

Two alignment pins were added to the sub-stage to align the ports of the sub-stage and the chip. The pins also aligned the pressure plate to the overall structure. Additionally, a cushioning material was adhered to the pressure plate to ensure that pressure was applied only to areas of the chip that were supported underneath. This would reduce deforming stresses on the chip when it was clamped.

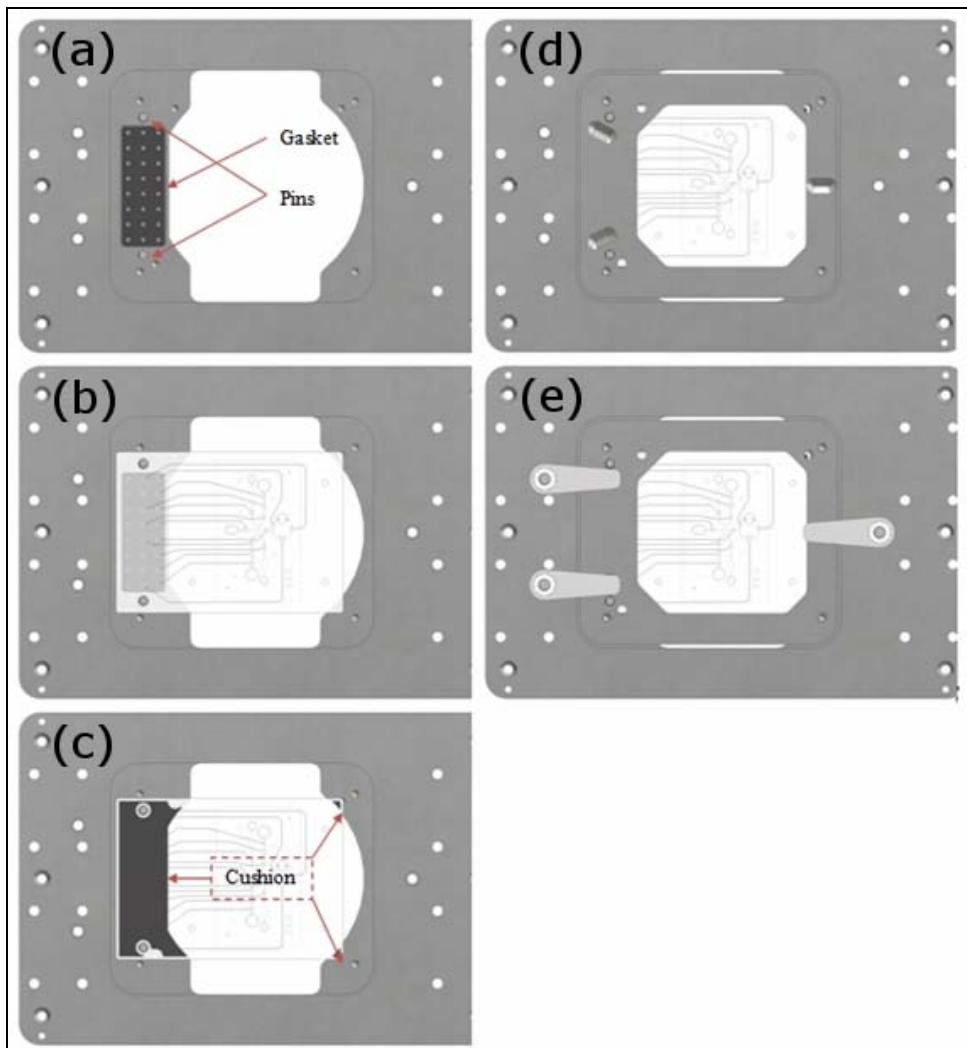


Figure 13 Layers of the redesigned substage system: (a) sub-stage base, (b) base with chip, (c) base with chip and rubber cushion, (d) placement of pressure plate, (e) placement of clamps to hold pressure plate in place.

When implemented, this new design was found to have some flaws of its own. The pneumatic sealing was inconsistent from one microfluidic chip to another. The clamps were difficult to manipulate, due to size and stiffness, and the shafts occasionally loosened from the sub-stage. Finally, the system sealed best when the pressure plate was without the cushioning material. In order to correct these issues a further revision was implemented.

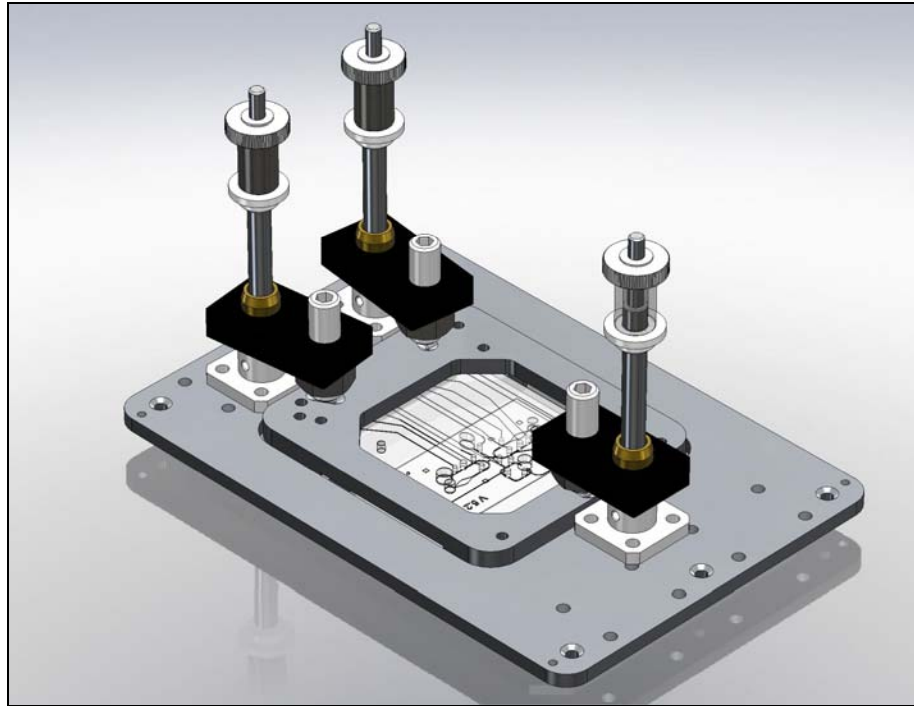


Figure 14 Current sub-stage design, showing clamp placement (springs not shown)

The second revision applied a number of adjustments to the preceding design. The position of the gasket was modified so it would seal with higher pressure, 5.4 psi. The springs were changed to apply this new pressure. The linear shafts were given sturdier shaft supports to keep them firmly in place. Bushings were added to the clamps to keep them from sticking along the shafts. The size of the clamp bodies was increased to enable easier handling. The bottom of the pressure plate was machined so it would only touch the chip where the chip was supported underneath, which obviated the need for the cushioning material shown in Figure 13c. The current substage design is shown in Figure 14.

To compare the degree of focus drift with the current substage design with that of the older, pneumatic-clamp substage, a small number ($n=4$) of microfluidic chips were tested. Each chip was placed in the current substage, and the displacement of the bottom surface was measured every 20 minutes over the course of one hour. Displacement was measured by refocusing the microscope on the bottom surface and noting the change in focal position. Figure 15 displays the measurements, along with a linear fit to the data from all four chips. The characteristic drift observed for the pneumatic-clamp substage, which had been previously measured, is also shown for comparison. These data indicate that focus

drift on the new substage is, on average, half as great as on the pneumatic-clamp substage.

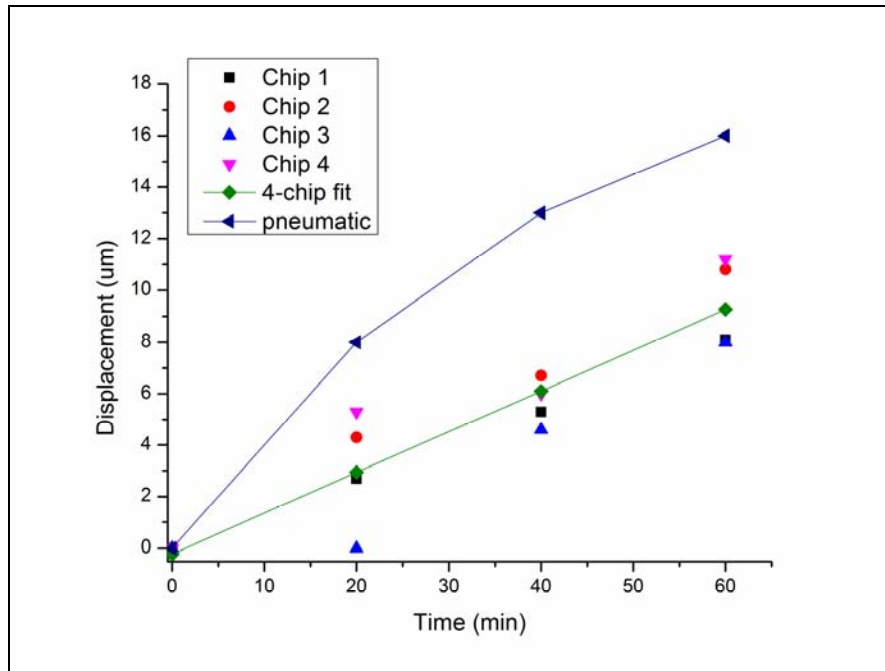


Figure 15 Pressure-induced focus drift for four microfluidic chips held in the revised sub-stage (shown in Figure 14), compared to the drift for the older pneumatically-clamped design (shown in Figure 11).

3.3 Automated Sperm Identification under Bright Field Illumination

During our previous development phase, computer identification of sperm was aided by the use of fluorescence microscopy. A fluorescent intercalating dye was introduced to the elute, prior to inspection. This dye, propidium iodide, tagged the nuclei of the cells present in the sample, including the sperm. Inspection of the sample was performed using standard fluorescence microscopy techniques. In the resulting images, cells appeared as bright red spots on a black background, and sperm were distinguished from epithelial cells on the basis of spot size. Figure 16 shows an example of such a fluorescence image produced by our equipment.

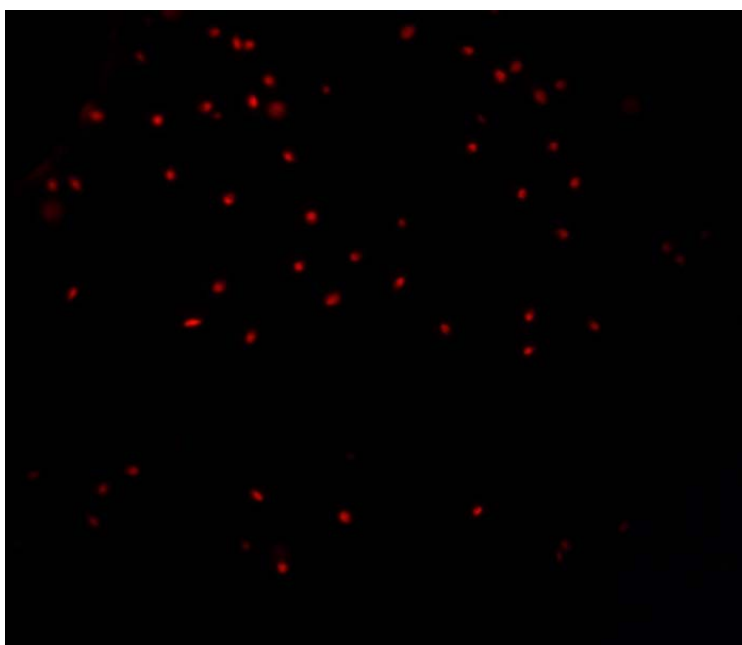


Figure 16 Fluorescence image of sperm dyed with propidium iodide.

The use of fluorescent dye greatly simplified the image analysis problem, and enabled us to work on the processes for trapping and moving sperm without first developing and testing more complex image analysis methods.¹² However, the ultimate goal of this development project has been to create a commercially viable system that can be deployed to forensics labs that possess varied levels of resources, and that have their own established workflows and procedures. Requiring the use of a particular fluorescent dye with our system promised to be problematic for several reasons. First, dying the cells eluted from an evidence swab adds additional steps to the processing of evidence, which is contrary to the goal of simplifying the analysis of sexual assault evidence swabs. Second, intercalating nuclear dyes such as propidium iodide are known mutagens, and thus their use requires lab technicians to take extra care and may require labs to put extra safety procedures in place if such dyes are not regularly used in current workflows. Third, various labs have pre-existing preferred methods and dyes for staining sperm, which might not be compatible with our recommended methods. Finally, the addition of

fluorescence microscopy capabilities would raise the cost of any eventual commercial device.

Therefore, in order to avoid these potential difficulties, it was necessary to design and implement image analysis methods that would enable identification of sperm using ordinary bright-field microscopy, without the use of fluorescent dyes. Identification of sperm in images obtained under bright field illumination is more challenging than the same task in the case of fluorescence images. In the fluorescence images, thanks to the selective labeling of objects containing DNA, it is relatively straightforward to locate and analyze all of the bright spots which may be sperm cells. In the case of brightfield illumination, all other physical objects present on the surface are visible. These other objects may have size and structure similar to sperm cells. Furthermore, any surface defects such as scratches and other artifacts are visible and contribute to the complexity of object identification. Finally, how a microscopic object--such as a sperm cell--appear in an image can vary dramatically, depending on its vertical position relative to the imaging plane of the microscope's objective lens. These last two factors necessitated the hardware improvements documented in Sections 3.1 and 3.2.

3.3.1 Identification of Best Focal Plane

The variation in sperm appearance in different focal planes presents a challenge, but with good hardware control, it also provides the opportunity to improve particle identification by selecting a focal plane where the sperm have the most distinctive appearance. Figure 17 contains examples of brightfield images of a sperm and corresponding intensity profiles taken along the line superimposed on each image. Every line profile consists of three RGB components (red, green and blue). The images are taken at different focal planes above the surface where the sperm are located, starting at $Z = 0 \mu\text{m}$ (i.e. the lower surface of the sample channel) and ending at $Z = 11 \mu\text{m}$ above the lower surface. Visual inspection of the images indicates that as the focal plane moves up from the initial position, the image of sperm becomes brighter and sharper up to approximately $Z = 7 \mu\text{m}$. Beyond that, as the height of the imaging plane continues to increase, the image becomes darker and more blurred. This observation can be expressed quantitatively by measuring the peak-to-background ratio of the main peak corresponding to the bright spot in the sperm of the line profiles corresponding to each image. This ratio has the largest value for the sharpest image. This suggests that the best images of sperm can be acquired by setting the focal plane around 6 or 7 μm above the surface and identified by looking for bright objects in the images taken.

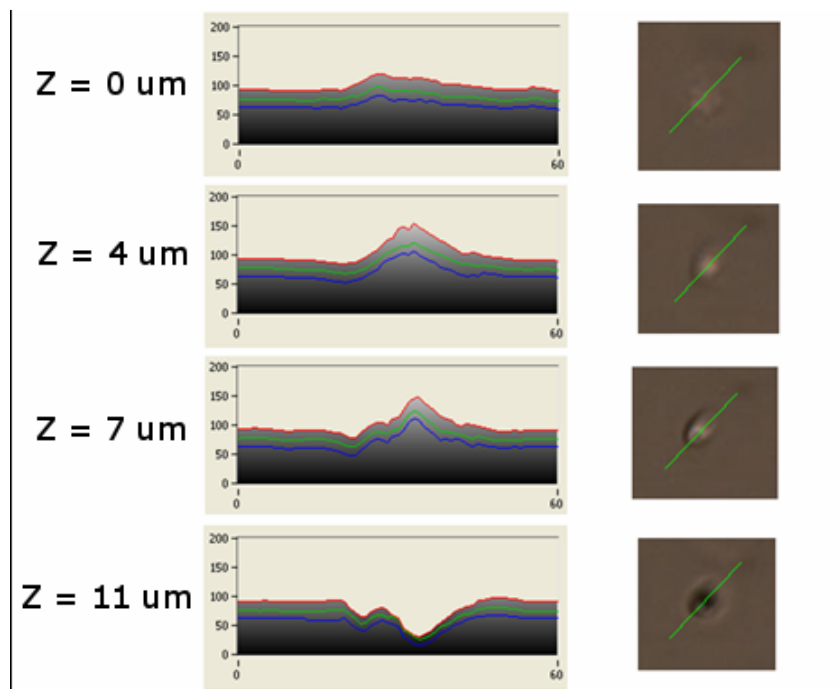


Figure 17 Examples of sperm images taken at different positions above the lower surface of the microfluidic channel, and the corresponding line profiles taken along the green line shown on each image. $Z = 0 \mu\text{m}$ corresponds to the bottom surface of the channel.

3.3.2 Locally Adaptive Thresholding

The concept of local thresholding, also known as locally adaptive thresholding, for particle identification is based on calculating a local pixel intensity statistic, such as range, variance, surface fitting parameters, or one of their logical combinations for each pixel in an image. The result of this calculation is the so-called Local Threshold Value which characterizes each pixel. Several algorithms exist which use various criteria to compare the original pixel intensity with its local threshold value and determine whether the pixel under consideration belongs to a feature (particle) or to the background. As an initial attempt at sperm identification, we used two common methods that are implemented as part of the NI Vision 2010 package for LabVIEW. These are the Niblack and the Background Correction algorithms.²⁹

These algorithms were tested on a set of 40 images of sperm cells located on the surface of a COC-molded microchannel. All images were obtained in the “bright object” mode, i.e. sperm centers or at least some parts appear as bright spots. Both algorithms produced similar results: they work very well in most cases but often they failed completely for no discernable reason. Using the background correction method on the 40 images, there were 12 complete failures. This represents a success rate of 70 % (28/40). The performance of the Niblack algorithm was better, but still resulted in some spectacular failures. Figures 18 and 19 show one example of successful identification and one example of failure, respectively. The relatively low success rate for the stock NI Vision local-thresholding methods is insufficient for automated processing of a swab elute, and thus it was necessary to consider other approaches.

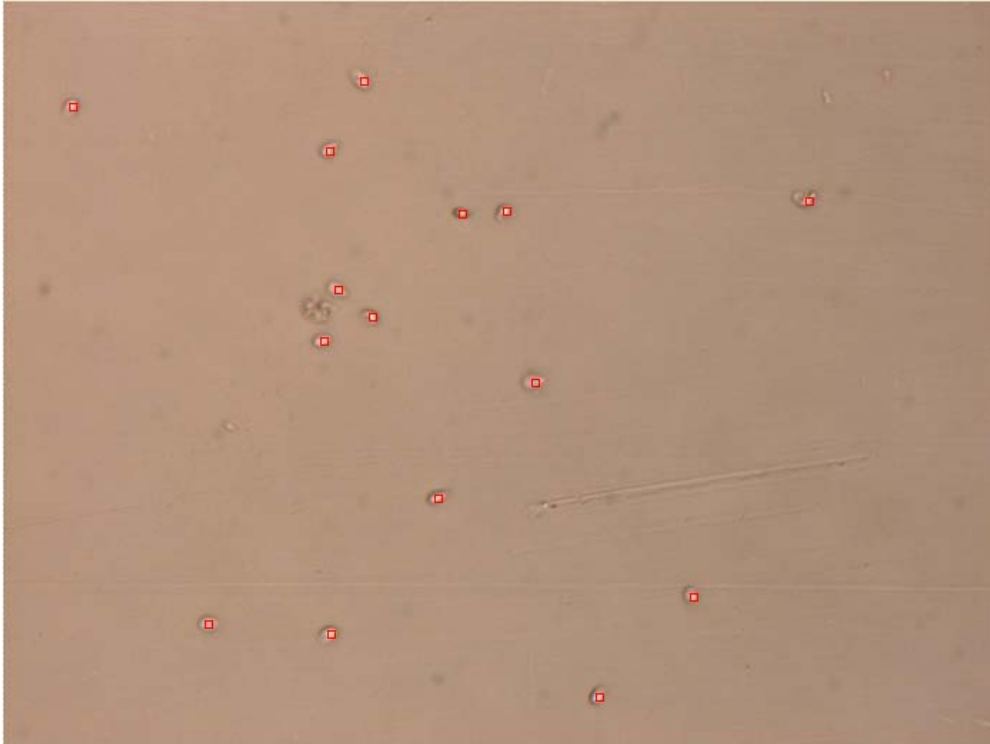


Figure 18 Example of successful sperm identification with the use of the Background Correction algorithm. Red squares represent positions where the algorithm found sperm. All 15 sperm cells were identified correctly.

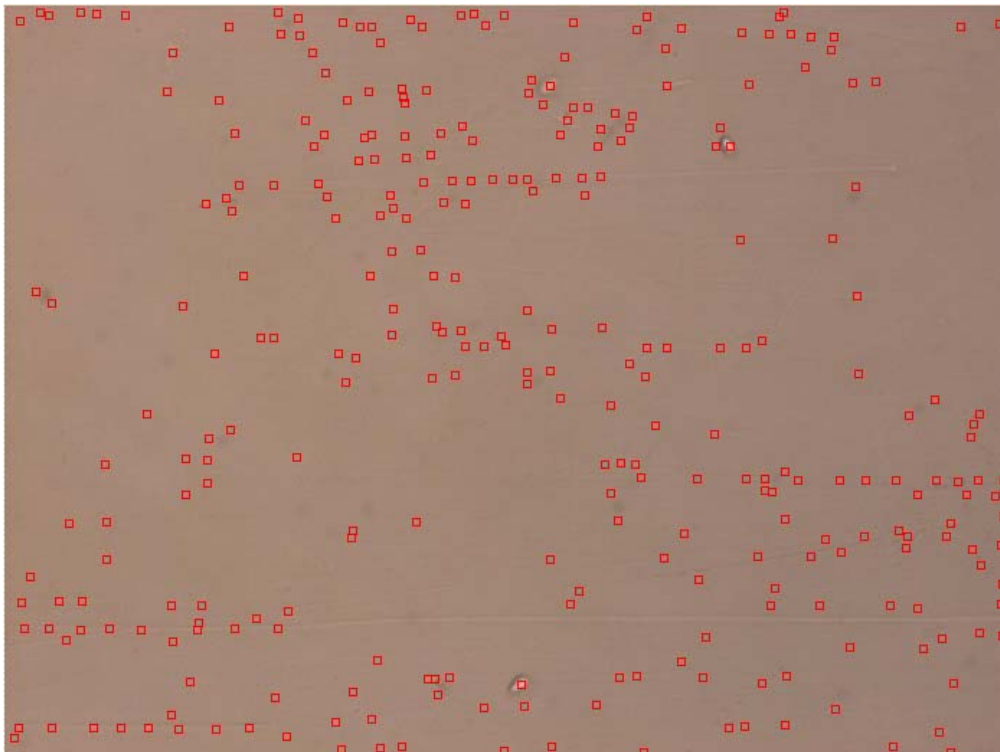


Figure 19 Example of the failure of sperm identification with the use of the Background Correction algorithm. In addition to three correctly identified sperm cells, the algorithm produced 295 false sperm identifications, where no object was present.

3.3.3 “Three Sigma” Background Correction

Due to the unsuitable performance of the local thresholding methods of bright object identification, it was necessary to implement a technique that would perform better under varying backgrounds and image intensities. The objective was to find a reliable method of automated calculation of threshold limits for the range of pixel intensities to be included in the search for bright objects (sperm), based on the measurable properties of each image, without additional assumptions about illumination uniformity or surface morphology such as scratches, other defects, and non-sperm material. As a first step toward this goal, histograms of sample images containing sperm were studied.

Figure 20 contains a histogram of the image from Figure 5, which contains 15 sperm cells. The graph shows the number of pixels of a given intensity, as a function of the intensity which is the 8-bit gray scale number between 0 and 255. The intensity distribution centered around the value of $I=177$ represents the image background. If the image contained only a uniform background, this peak would look very much like an ideal Gaussian distribution. Additional “fine structure” visible in the peak is due to “imperfections” in what would be a smooth background, i.e. sperm cells and surface defects.

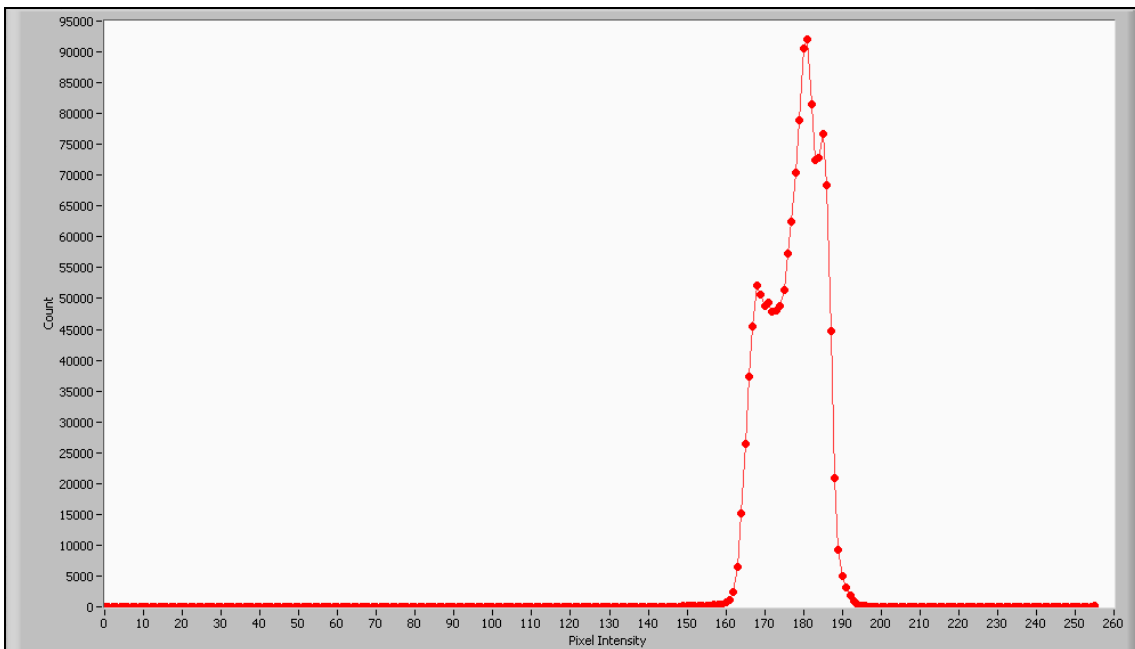


Figure 20 Pixel-intensity histogram for the image of Figure 5, which contains 15 sperm

Information about all non-background objects is also hidden in the tails of the distribution, on the lower-intensity side for dark objects, and on the higher-intensity side for bright objects. This can be clearly seen in Figure 21, which shows the same histogram as Figure 20, zoomed in on the low-count tail area. The tail shapes clearly deviate from the standard Gaussian distribution. It is reasonable to postulate that most such deviations on the high-intensity side correspond to bright features in the image. Thus, since the high limit of the intensity range is 255, it is only necessary to devise a method of calculating the low limit, shown approximately in Figure 21 as “LL.”

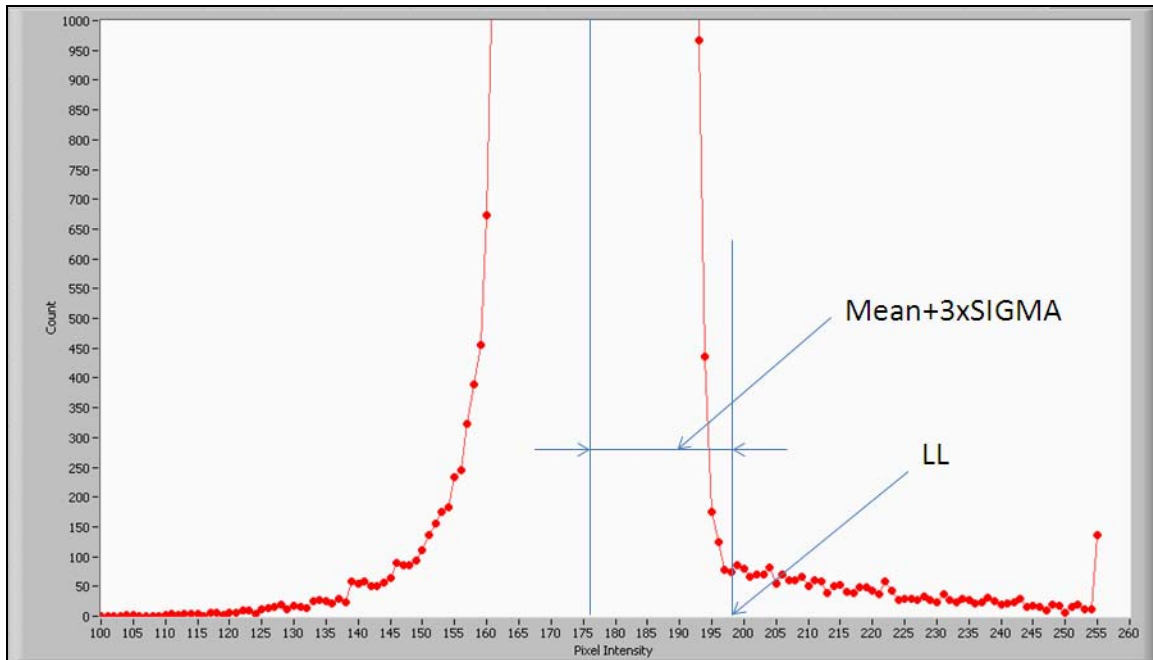


Figure 21 Zoomed-in view of histogram of the image in Figure 20, concentrating on low-count values. Deviation of the graph from the Gaussian shape clearly visible at both low and high intensity tail areas. LL represents approximately the intensity above which all pixels belong to the bright objects in the image.

The numerical value of “LL” for a given image is estimated by calculating the mean and standard deviation of the image’s pixel intensity values, and approximating the histogram by a Gaussian distribution with the same mean and standard deviation. Because 99% of a Gaussian distribution lies within three standard deviations of the mean, the value of LL is taken to be the mean plus three standard deviations. Pixels with intensities higher than this cutoff are selected as candidates for belonging to image features that represent sperm. Particle identification then proceeds according to standard methods for identifying bright objects.^{12, 29, 30}

This “three sigma” technique shows improvement over the basic local thresholding methods for the images we have tested it on, specifically, the 40-image set that was used to evaluate the background correction methods. For example, Figure 9 shows the results for the histogram-analysis method for the image of Figure 3. Unlike the background correction algorithm, this histogram-analysis method results in correct identification of all the sperm cells, and there are no spurious identifications.



Figure 22 The same image as in Figure 3, analyzed using the “three sigma” histogram-correction method. Sperm cells are correctly identified, and there are no false identifications.

3.3.4 Distinguishing Sperm from Yeast

Yeast naturally grows in the human vagina, and is thus frequently present in vaginal swabs taken from sexual assault victims. Yeast cells vary in size, and may appear similar to tailless sperm in bright-field (or fluorescence) microscope images. The presence of yeast DNA does not interfere with STR analysis for human identification, because human-specific primers are used for the PCR amplification. However, the presence of yeast presents some challenges for our HOT-based sperm isolation system. If the computer image analysis selects yeast as well as sperm for isolation, then the number of actual sperm in the output area will be lower than a particle count indicates. This, in turn, means that a larger number of particles must be selected if a sufficient quantity of sperm DNA is to be recovered for STR analysis, and thus the total processing time will be longer. Furthermore, an inability to distinguish sperm from yeast means that any attempt at counting the number of isolated sperm for DNA quantitation purposes will be doomed to failure. We therefore found it necessary to examine mixtures of yeast and sperm in order to formulate a method for distinguishing the two types of cells.

Before proceeding, two caveats should be noted. First, the sperm-and-yeast swabs provided to us by Orchid-Cellmark contain baker’s yeast (*Saccharomyces cerevisiae*), not the *candida* yeast that is present in the human vagina. We did not have access to swabs containing *candida*. Second, all of the particular measurements and observations we made are specific to our current hardware configuration. Therefore, the results described below should be taken as an example of a process for deriving a test for distinguishing

images of yeast from images of tailless sperm, rather than as a formula that can be applied without further consideration.

Figure 23 shows a microscope field of view containing sperm and yeast eluted from a swab. On the whole, these yeast cells are larger and rounder than the sperm cells, but using the “three sigma” thresholding method described in Section 3.3, along with an area-based criterion for selecting sperm resulted in misidentification of several yeast cells as sperm, or in some cases as two sperm. Of the 24 features identified as sperm, only 12 were truly sperm.

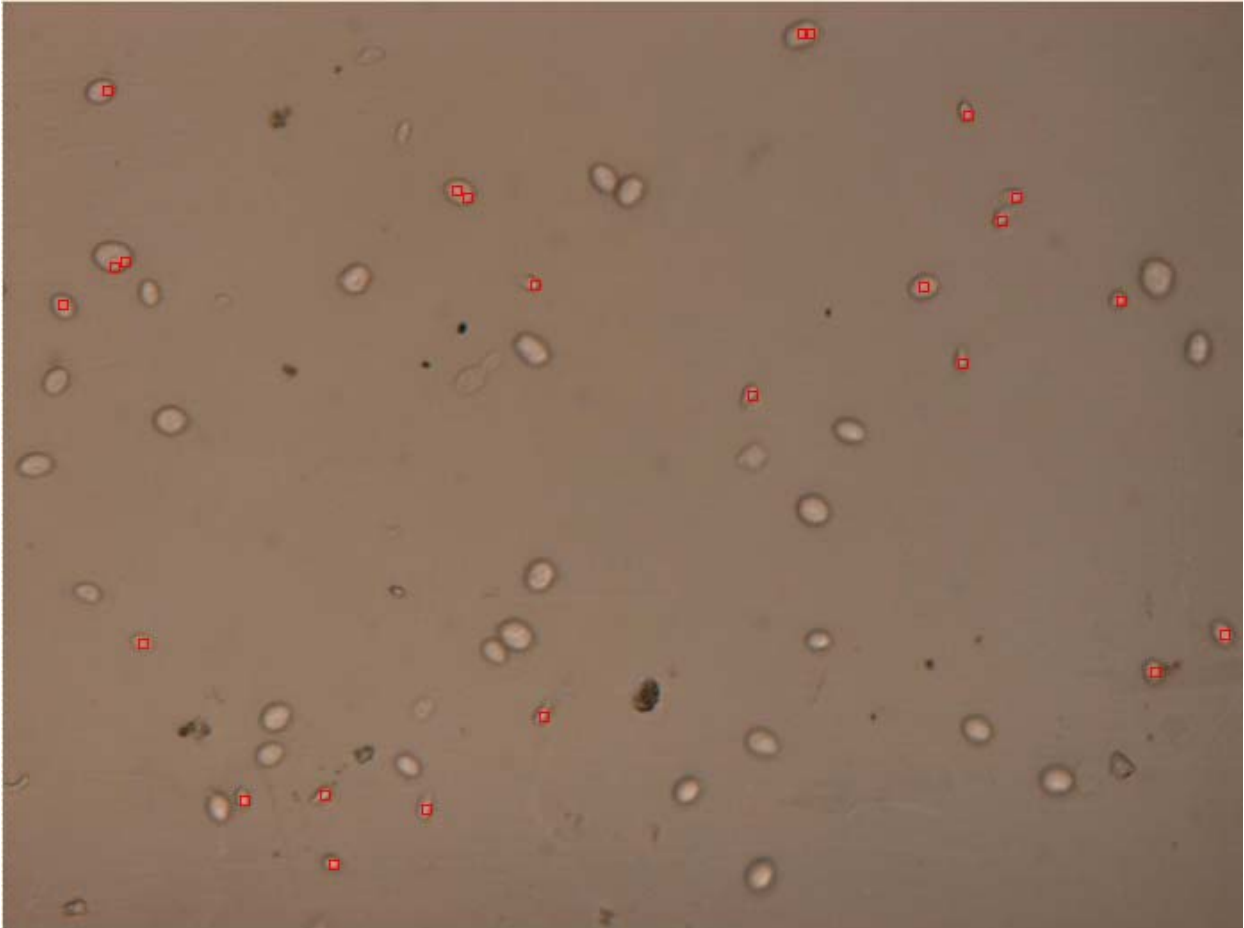


Figure 23 Microscope field of view containing yeast and sperm cells. The red squares indicate features that were identified as sperm when using the “three sigma” thresholding method and an area-based selection criterion.

Since particle size alone is an insufficient for distinguishing sperm from yeast, it is necessary to employ one or more shape-based criteria. As a prerequisite, it is necessary to extract the “shape” of a feature from the image. We used the following approach, implemented using National Instruments NI Vision 2010 package for LabVIEW.

This procedure is applied to all features tentatively identified as “sperm” in an image:

1. Select a subregion of the image containing the feature in question plus its local background
2. Improve contrast by applying a look-up table. In our case, we used NI Vision 2010's Lookup Table 1
3. Convert the image to binary by applying an automatic threshold²⁹
4. Apply feature-separation algorithm³¹
5. Apply watershed segmentation³² to extract the particle shape
6. Calculate particle-shape metrics for the particle. These metrics can be used to distinguish yeast and sperm cells.

Two examples of this procedure, applied to one sperm and one yeast cell, are shown in Figures 24 and 25. In both cases, the central red area is the region identified as the particle of interest. Comparing the segmentations to the original images, one can see that the shapes derived through watershed segmentation match the object appearance quite well. The segmentation-derived shape is used to calculate area, perimeter, and combinations thereof which are used as shape metrics. These shape metrics, in turn, are employed to distinguish the two cell types.

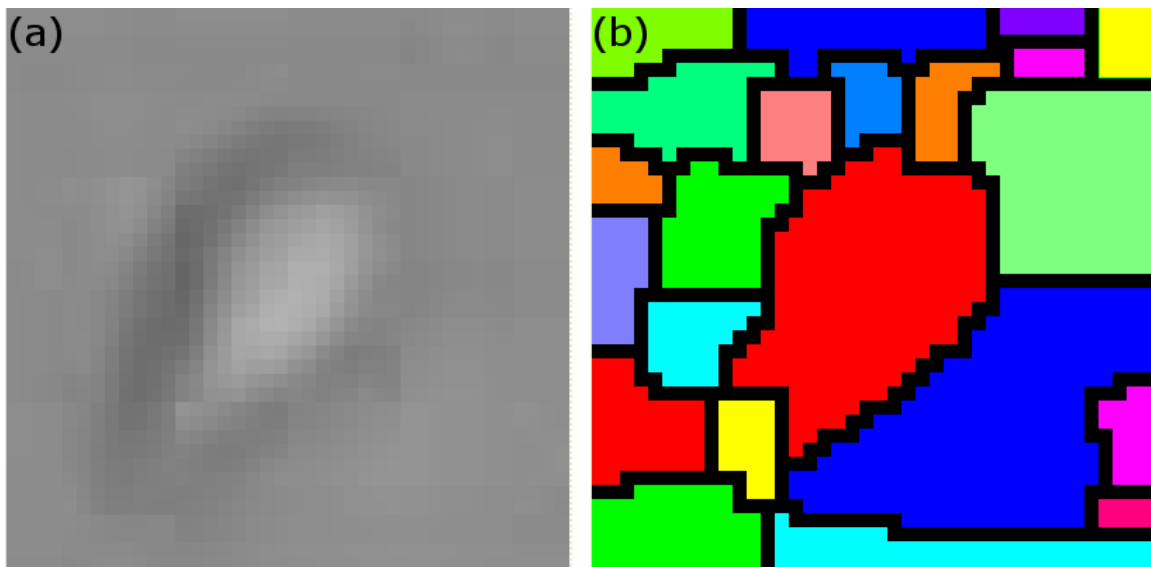


Figure 24 (a) A 40 x 40 pixel image of a sperm cell, extracted from the image of Figure 23. **(b)** Watershed segmentation of the image, used to define the “shape” of the feature of interest.

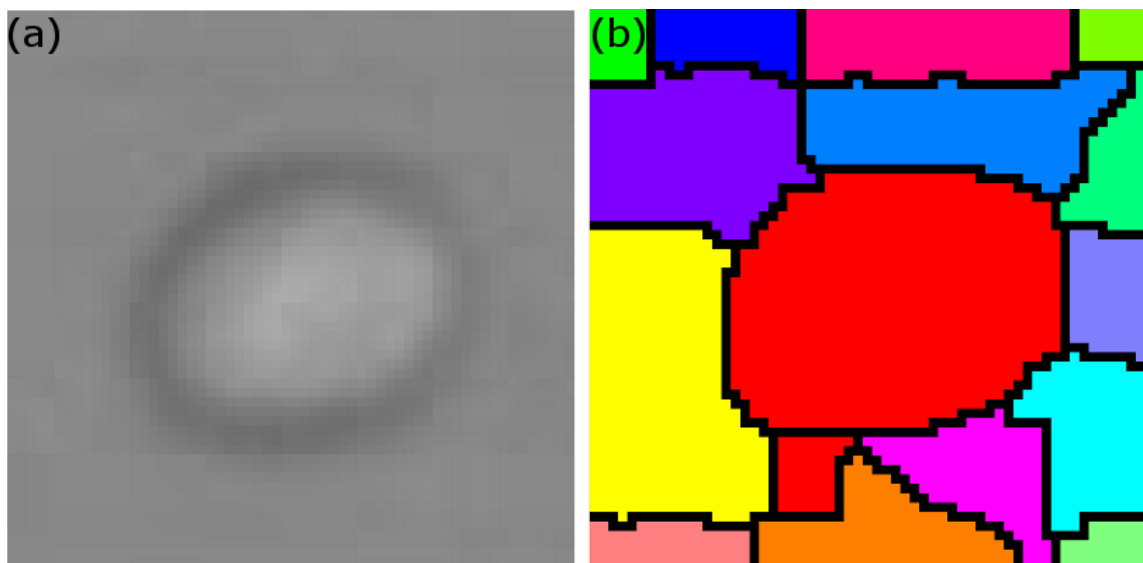


Figure 25 (a) A 60 x 60 pixel image of a yeast cell, extracted from the image of Figure 23. **(b)** Watershed segmentation of the image.

We considered the following parameters:

- Hydraulic radius: this is the area of the shape, divided by its perimeter
- Waddell Disk Diameter: this is the diameter of a circle with the same area as the particle
- Ratio of equivalent ellipse axes: this is the ratio of major axis to minor axis lengths of an ellipse that has the same area and same perimeter as the shape
- Elongation factor: this is the ratio of the largest distance between any two points in the shape to the length of the short side of a rectangle having the same area and same perimeter as the shape
- Heywood circularity factor: this is the perimeter of the shape, divided by the circumference of a circle of the same area. It is a measure of circularity
- Area: the number of pixels in the shape

We applied the Welch two-sample t-test to determine whether there was a statistically significant difference between the means of these parameters for the sperm and yeast images in Figure 23. The attained significance levels (p-values) for the tests are listed in Table 1, along with the means and standard deviations. All six quantities were found to have significantly different means, judged at the $\alpha=0.05$ significance level.

Figure 26 contains box plots showing the distributions of values for these quantities for the 24 features (12 sperm and 12 yeast) identified in Figure 23. In each of these plots, the box represents the range between the first and third quartiles, the thick line inside the box is the median, and the “whiskers” represent values within 1.5 times length of the box. Outliers are represented by standalone dots. Even if the outlying point is discounted, it is clear that although the mean values for these quantities may differ significantly between yeast and sperm, there is significant overlap between the observed ranges for the two particle types. Therefore, using only one parameter to make a judgment regarding whether a particle is sperm or yeast is unlikely to prove successful.

Table 1 Particle Characterization Parameters: Means, Standard Deviations, and Attained Significance Level (p-value) for a t-test for Difference of Means between Sperm and Yeast

Parameter	Cell Type	Mean	Std Dev	p-value of t-test for Difference of Means
Hydrodynamic Radius	Sperm	4.53	0.50	<0.0001
	Yeast	7.47	1.10	
Waddell Disk Diameter	Sperm	20.4	2.0	<0.0001
	Yeast	32.1	5.1	
Ratio of Equiv. Ellipse Axes	Sperm	2.06	0.43	0.025
	Yeast	1.71	0.13	
Elongation Factor	Sperm	2.34	0.50	0.011
	Yeast	1.87	0.14	
Heywood Circularity Factor	Sperm	1.13	0.07	0.023
	Yeast	1.07	0.02	
Area	Sperm	331	65	<0.0001
	Yeast	829	256	

The outlying point seen in Figures 26a, 26b, and 26f was not included in the data used in the t-tests to determine whether the means of the parameters differed between yeast and sperm. This is justified by the fact that in practice, any image feature that was such a clear outlier would be rejected as a candidate for optical-trapping-based isolation.

Of course, we do not consider data from one image to be sufficient to derive a mathematical model for differentiating sperm from yeast. The above analysis of Figure 23 should be taken as an example only. To develop a truly reliable model, one would obtain many images, preferably using different samples and different microfluidic chips, and perform a similar statistical analysis on the set of all particles identified as potential sperm in all of the images. Once the statistically significant parameters were identified, they could be used to formulate a logistic regression model for differentiating the two cell types. The reasons why we cannot present such a thorough analysis are discussed in Section 4.2.

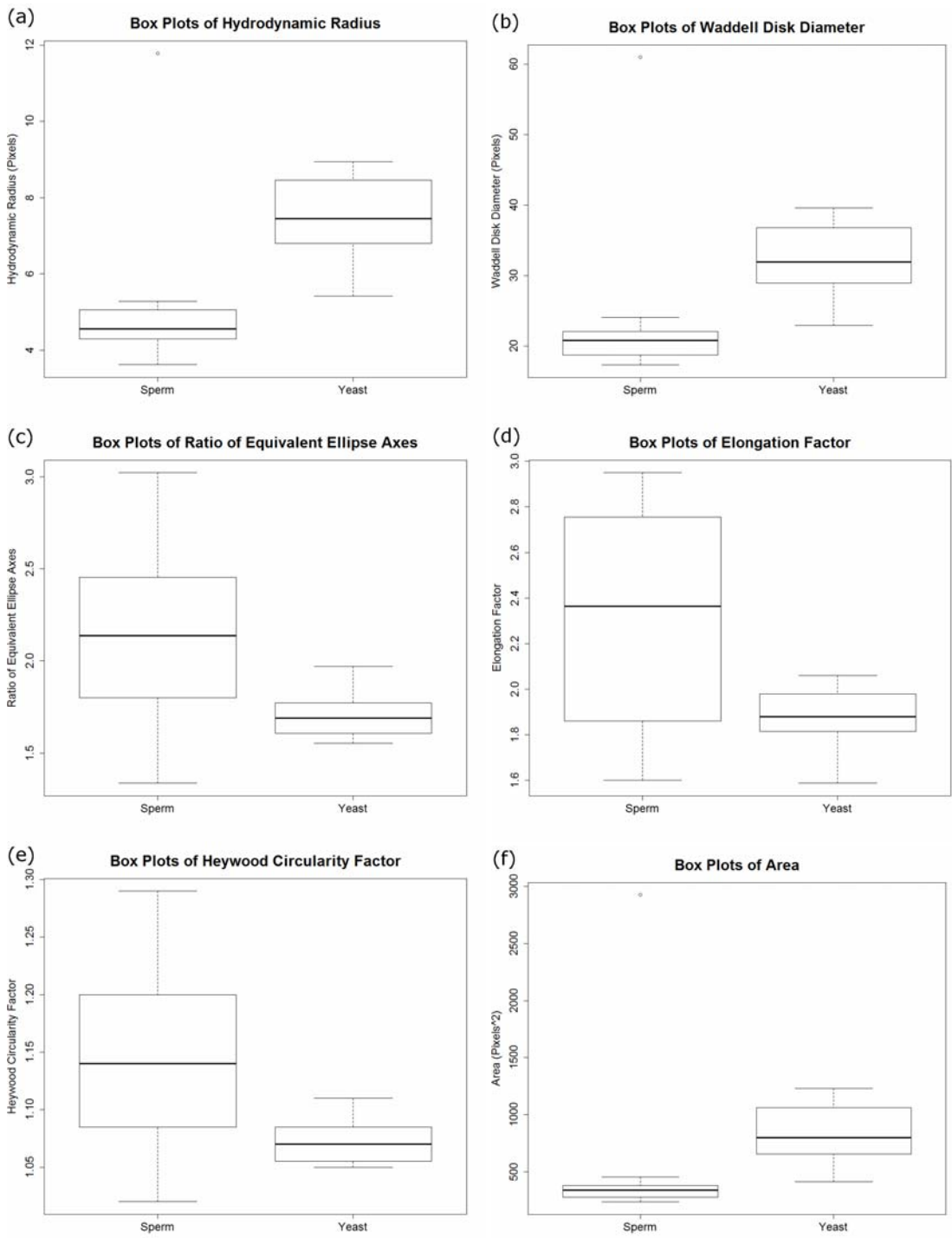


Figure 26 Box plots showing the distributions of the shape parameters used to distinguish similarly-sized yeast and sperm. In each plot, the thick black line represents the median value. The box represents the first and third quartiles, and the “whiskers” represent values lying within 1.5 times the box width of the box boundaries. Outliers are represented by free-standing dots.

4 Conclusions

4.1 Summary and Discussion of Results

As laid out in Section 1.3, one major objective for the research phase covered by this report were to develop methods for computer identification of human sperm eluted from a sexual assault evidence swab under bright-field microscopy. These methods, along with associated hardware improvements, were to be implemented on our automated holographic optical trapping device for isolating sperm from other components of the elute. The other objective was to investigate the potential for using the imaging techniques to complement or improve upon current DNA quantitation techniques by counting the number of sperm in the output area of the device.

The hardware challenges proved to be more important than we had anticipated, and thus required a greater proportion of resources and time to resolve. The ability to acquire consistent high-quality images is a prerequisite for reliable image analysis. When we moved from glass-bottomed microfluidic chips to chips with COC-molded channels, the optical quality of the COC channels was mediocre. It took several design iterations to obtain a satisfactory manufacturing process for the mold from which the chips were made. In the final process, the mold was machined from one-inch thick surface-ground blocks of Alumold 500 aluminum, and polished to an optical finish using techniques derived from Reference 28. The fluidic channels produced from these molds had acceptable optical clarity and were largely free from scratches and other artifacts that could interfere with imaging.

In addition to creating optically clear microfluidic chips, we had to correct a problem with our automated microscopy system, where the imaging plane of the microscope tended to systematically drift away from the lower surface of the channels over time. The cause of this effect was determined to be an excess of clamping force used to hold the chip in place and couple it to the pneumatic system for controlling the microfluidic valves. This force caused the acrylic body of the chip to deform over time, resulting in vertical displacement of the fluidic channels relative to the imaging plane. An entirely new clamping system was designed and built, which exerted considerably less force on the chip. When the new clamping system was used, the focus was still found to drift over time, but at one half the rate that had been previously observed.

Once these hardware challenges were addressed to our satisfaction, we were able to proceed with acquiring good bright-field images of eluted sperm and developing image-analysis software techniques for identifying sperm and distinguishing it from other particles that might be found on a sexual assault evidence swab, such as yeast. First, we identified the optimal focal position, relative to the channel bottom, for imaging sperm. Then, using images containing sperm only, we developed a means of analyzing the intensity histogram of an image to set a thresholding level for locating bright objects in the field of view. Finally, we analyzed images of sperm cells and yeast cells and identified morphological parameters that can be used to distinguish sperm from similarly-sized yeast.

Unfortunately, we were not able to progress further with the image analysis work, or to implement the next step of attempting DNA quantitation through image analysis, because our research and development program was terminated prior to the end of the funding period.

4.2 Implications for Policy and Practice

Our informal discussions with forensic scientists suggest that there is a great deal of interest in the prospect of an automated device for high-purity sperm isolation from sexual assault evidence. A device that is sufficiently fast and affordable would reduce or eliminate the need for differential extraction, which in turn would improve lab efficiency by freeing workers for other tasks. The capability to observe a sample throughout its processing would allow for improved and automated record-keeping. Knowing the number of sperm cells that have been isolated, and which are to be used for STR profiling would enable more precise estimation of the optimal quantity of PCR reagents needed, and thus improve the probability of obtaining a good result.

The main technical limitations on our research were hardware and sample related. Over the course of the current research phase, it has become clear that we have reached the limit of our present hardware's capabilities. This hardware—the automated holographic optical trapping system and microfluidic system described in Section 2.1.2-- had originally been developed as a general-purpose instrument, with adaptations made over time to address issues specific to the sperm isolation problem. Any significant further progress towards a commercial device would require production of a second-generation instrument designed with the forensic application in mind. We had, in fact, begun this process, although it was put on hold for business-related reasons.

Regarding limitations due to samples, all of our work to date has used mock forensic swabs supplied by Orchid-Cellmark. These swabs contain sperm, sperm and yeast, or sperm and epithelial cells, and have sufficed for early-phase development. However, these mock swabs are not necessarily characteristic of real evidence swabs collected from sexual assault victims. The most obvious difference is that real evidences swabs are collected from a victim's body, and are thus likely to contain a wider variety of contaminants than samples produced under controlled laboratory conditions.

Beyond technical limitations, the results of the project, and our ability to address our initial goals, were hampered by the fact that our research program has been terminated and our division closed. The final decision was made in early 2013, but it was preceded by the ending of other projects being pursued by Arryx, and the transfer of another project to a different division of our parent company. The effect of these business decisions on our project was a sharp reduction in resources and personnel we could call on to support our own work. In particular, layoffs, transfers, and voluntary separation of biology, chemistry, and engineering personnel made it impossible to pursue the DNA quantitation objectives laid out in the grant proposal, and increased the time and expenditure (due to the need to outsource tasks previously handled in-house) required for

hardware improvements which were prerequisites for the image-analysis objectives of our program. In turn, this slowed progress on image analysis. The cumulative effect was that we were able to accomplish considerably less than we had envisioned when our proposal was submitted to the NIH in 2011.

4.3 Implications for Further Research

Although we will not be continuing this research program ourselves, we present here some recommendations and suggestions for future researchers who may wish to pursue similar work.

Development of a robust computer-vision method for identifying sperm eluted from an evidence swab is aided by having a solid, reliable hardware platform. As was previously mentioned, if we were to have continued this project, one of the first objectives would have been to design and produce a new, integrated hardware system that was designed specifically for the sperm-isolation application. Such a device would have enabled us to partner with a working forensics laboratory, thereby gaining insight into laboratory workflows and the types of samples they typically encounter. This, in turn, would have informed the design and production of a commercial instrument.

The microfluidic chip is central to the sperm-isolation method, and it must have both good fluid-handling capabilities and good optical qualities. Our present chip design and manufacturing process is capable of producing chips of sufficiently high quality, but it suffers from a great deal of variability. That is to say, many of the chips produced in our laboratory have problems with flow or with optical quality. Further progress with our program would have required significant effort in standardizing the manufacturing process. We have also discovered that the composition of the buffer fluid plays a strong role in whether the eluted sperm and other material flow freely through the channels, or stick to the surfaces. This matter deserves further study.

Our work on developing image analysis routines for identifying sperm in bright field microscope images was in its early stages when work was stopped. The example in Section 3.4 of distinguishing sperm from yeast points the way towards development of a more generally-applicable approach. The first step should be acquiring a large number of images of sperm alone, yeast alone, epithelial cells alone, and images of mixtures of those components. By analyzing these images using an approach similar to that of Section 3.4, one could identify the combination of morphological parameters that is most effective in identifying sperm. A necessary part of any such analysis would be identification of outlier image features, and rejection of such outliers from consideration as potential sperm. It may prove to be the case that the best approach is to use a combination of bright field imaging and fluorescence imaging to identify all components of interest in a swab elute.

A final step would be to implement holographic optical trapping to trap and move sperm identified by a reliable sperm-recognition routine. The sperm thus isolated could be counted, extracted, and then subjected to traditional DNA quantitation methods. This

would provide valuable insight into the possibility of supplementing traditional quantitation with sperm counts in order to better estimate the quantity of PCR reagents to be used in amplification prior to STR analysis.

5 References

- ¹ Applied Biosystems, “Why Use Y?,” accessed October 12, 2011, [http://marketing.appliedbiosystems.com/mk/get/QUANTDUO_WHY_USE_Y.jsessionid=cc30faa54c07\\$AC\\$0D5Y?_A=97250&_D=62234&_V=0](http://marketing.appliedbiosystems.com/mk/get/QUANTDUO_WHY_USE_Y.jsessionid=cc30faa54c07AC0D5Y?_A=97250&_D=62234&_V=0).
- ² K. Coetzee, T. F. Kruger, and C. J. Lombard, “Repeatability and Variance Analysis on Multiple Computer-assisted (IVOS*) Sperm Morphology Readings,” *Andrologia* 31, no. 3 (1999): 163–168, doi:10.1111/j.1439-0272.1999.tb01404.x.
- ³ Kruger Tf et al., “A new computerized method of reading sperm morphology (strict criteria) is as efficient as technician reading.,” *Fertility and sterility* 59, no. 1 (January 1993): 202–209.
- ⁴ R Harr, “Characterization of Spermatozoa by Planar Morphometry,” *Clinical Laboratory Science: Journal of the American Society for Medical Technology* 10, no. 4 (August 1997): 190–196.
- ⁵ D L Duewer et al., “NIST Mixed Stain Studies #1 and #2: Interlaboratory Comparison of DNA Quantification Practice and Short Tandem Repeat Multiplex Performance with Multiple-source Samples.,” *Journal of Forensic Sciences* 46, no. 5 (n.d.): 1199–1210.
- ⁶ Margaret C. Kline et al., “NIST Mixed Stain Study 3: DNA Quantitation Accuracy and Its Influence on Short Tandem Repeat Multiplex Signal Intensity,” *Analytical Chemistry* 75, no. 10 (May 1, 2003): 2463–2469, doi:10.1021/ac026410i.
- ⁷ Andrew Hopwood et al., “A Fully Integrated Robotic System for High Sample Throughput Within a DNA Databasing Unit,” *Proceedings: LabAutomation '98* (1997): 17–21.
- ⁸ Applied Bio, “Quantifiler Human DNA Quantification Kit and Quantifiler Y Human Male DNA Quantification Kit User’s Manual,” 2003.
- ⁹ Janice A. Nicklas and Eric Buel, “Quantification of DNA in Forensic Samples,” *Analytical and Bioanalytical Chemistry* 376, no. 8 (August 1, 2003): 1160–1167, doi:10.1007/s00216-003-1924-z.
- ¹⁰ John C Fox, Christopher A Cave, and James W Schumm, “Development, Characterization, and Validation of a Sensitive Primate-specific Quantification Assay for Forensic Analysis,” *BioTechniques* 34, no. 2 (n.d.): 314–323.
- ¹¹ Tania Charkrabarty, “Final Technical Report for 2008-DN-BX-K123: Holographic Optical Trapping in Forensic Research and Development: Application to Rape Kit Analysis” (National Institute of Justice, January 2010).
- ¹² Tania Chakrabarty et al., “Development of an Automated Holographic Optical Trapping Method for Sexual Assault Evidence Kit Analysis” (Arryx, Inc., October 28, 2011).
- ¹³ National Institute of Justice, “DNA Evidence Backlogs: Forensic Casework,” February 16, 2011, <http://nij.gov/nij/topics/forensics/lab-operations/evidence-backlogs/forensic-evidence-backlog.htm>.
- ¹⁴ A Ashkin and JM Dziedzic, “Optical Trapping and Manipulation of Viruses and Bacteria,” *Science* 235, no. 4795 (March 20, 1987): 1517–1520, doi:10.1126/science.3547653.
- ¹⁵ Michael Sheetz, *Laser Tweezers in Cell Biology* (San Diego: Academic Press, 1998).

-
- ¹⁶ Jaelyn M Nascimento et al., “The Use of Optical Tweezers to Study Sperm Competition and Motility in Primates,” *Journal of The Royal Society Interface* 5, no. 20 (March 6, 2008): 297–302, doi:10.1098/rsif.2007.1118.
- ¹⁷ Furqan M Fazal and Steven M Block, “Optical Tweezers Study Life Under Tension,” *Nat Photon* 5, no. 6 (June 2011): 318–321, doi:10.1038/nphoton.2011.100.
- ¹⁸ Carlos Bustamante, Zev Bryant, and Steven B. Smith, “Ten Years of Tension: Single-molecule DNA Mechanics,” *Nature* 421, no. 6921 (January 23, 2003): 423–427, doi:10.1038/nature01405.
- ¹⁹ Eric R. Dufresne et al., “Computer-generated Holographic Optical Tweezer Arrays,” *Review of Scientific Instruments* 72 (2001): 1810, doi:10.1063/1.1344176.
- ²⁰ Jennifer E. Curtis, Brian A. Koss, and David G. Grier, “Dynamic Holographic Optical Tweezers,” *Optics Communications* 207, no. 1–6 (June 15, 2002): 169–175, doi:10.1016/S0030-4018(02)01524-9.
- ²¹ Boulder Nonlinear Systems, “XY Series Spatial Light Modulators Specification Sheet,” accessed October 26, 2011, <http://www.bnonlinear.com/products/xyslm/nematic.pdf>.
- ²² David Grier, “A Revolution in Optical Manipulation,” *Nature* no. 424 (August 14, 2003): 21–27.
- ²³ George M. Whitesides, “The Origins and the Future of Microfluidics,” *Nature* 442, no. 7101 (July 27, 2006): 368–373, doi:10.1038/nature05058.
- ²⁴ William H Grover et al., “Monolithic Membrane Valves and Diaphragm Pumps for Practical Large-scale Integration into Glass Microfluidic Devices,” *Sensors and Actuators B: Chemical* 89, no. 3 (April 1, 2003): 315–323, doi:10.1016/S0925-4005(02)00468-9.
- ²⁵ R Core Team (2012), *R: A Language and Environment for Statistical Computing* (Vienna, Austria: R Foundation for Statistical Computing, n.d.), <http://www.R-Project.org/>.
- ²⁶ Vijaya Sunkara et al., “Simple Room Temperature Bonding of Thermoplastics and Poly(dimethylsiloxane),” *Lab on a Chip* 11 (December 2010): 962–965.
- ²⁷ “Diamond Lapping, Honing, Grinding, Superabrasives--Engis Corp.,” accessed March 5, 2012, <http://www.engis.com/>.
- ²⁸ Victor Krottner, “How to Optically Polish Aluminum,” *MoldMaking Technology*, May 1, 2011, <http://www.moldmakingtechnology.com/articles/how-to-optically-polish-aluminum>.
- ²⁹ National Instruments, “Thresholding - NI Vision 2010 Concepts Help,” *NI Vision 2010 Concepts Help*, June 2010, <http://zone.ni.com/reference/en-XX/help/372916J-01/nivisionconcepts/thresholding/>.
- ³⁰ National Instruments, “Particle Measurements - NI Vision 2010 Concepts Help,” *NI Vision 2010 Concepts Help*, June 2010, http://zone.ni.com/reference/en-XX/help/372916J-01/nivisionconcepts/particle_measurements/.
- ³¹ National Instruments, “Advanced Morphology Operations - NI Vision 2010 Concepts Help,” *NI Vision 2010 Concepts Help*, June 2010, http://zone.ni.com/reference/en-XX/help/372916J-01/nivisionconcepts/advanced_morphology_operations/.
- ³² A.P. Mangan and R.T. Whitaker, “Partitioning 3D Surface Meshes Using Watershed Segmentation,” *IEEE Transactions on Visualization and Computer Graphics* 5, no. 4 (1999): 308–321, doi:10.1109/2945.817348.

6 Dissemination of Research Findings

The project funded by this award was presented at the following scientific conferences:

- **NIJ Conference 2012, Arlington, VA, June 18-20, 2012.** The principal investigator, Pamela Korda, and the lead software developer, Ryszard Duszak, presented a poster, entitled “Developing an Automated Device for High-Purity Sperm Isolation from Sexual Assault Evidence.”
- **Green Mountain DNA Conference, Burlington, VT, August 1-3, 2012.** The program manager, Dan Mueth, gave an invited talk, entitled “Development of an Automated Holographic Optical Trapping Method for Sexual Assault Evidence Analysis,” on August 2. The Green Mountain DNA Conference is an annual event, organized by the Vermont Forensics Laboratory.
- **SLAS2013, Orlando, FL, January 12-16.** The program manager, Dan Mueth, gave a podium presentation, entitled, “A New Platform for Cell Fractionation and its Application in Processing Forensic Samples.” SLAS is the annual meeting of the Society for Laboratory Automation and Screening.